The search for high entropy alloys: a high-throughput *ab-initio* approach

Yoav Lederer,[1,2] Cormac Toher,[1] Kenneth S. Vecchio,[3] and Stefano Curtarolo[4,5,*]

[1] *Department of Mechanical Engineering and Materials Science, Duke University, Durham, North Carolina 27708, USA*
[2] *Department of Physics, NRCN, Beer-Sheva, 84190, Israel*
[3] *Department of NanoEngineering, University of California San Diego, La Jolla, CA 92093*
[4] *Materials Science, Electrical Engineering, Physics and Chemistry, Duke University, Durham NC, 27708*
[5] *Fritz-Haber-Institut der Max-Planck-Gesellschaft, 14195 Berlin-Dahlem, Germany*

(Dated: July 16, 2018)

While the ongoing search to discover new high-entropy systems is slowly expanding beyond metals, a rational and effective method for predicting *"in silico"* the solid solution forming ability of multi-component systems remains yet to be developed. In this article, we propose a novel high-throughput approach, called "LTVC", for estimating the transition temperature of a solid solution: *ab-initio* energies are incorporated into a mean field statistical mechanical model where an order parameter follows the evolution of disorder. The LTVC method is corroborated by Monte Carlo simulations and the results from the current most reliable data for binary, ternary, quaternary and quinary systems (96.6%; 90.7%; 100% and 100%, of correct solid solution predictions, respectively). By scanning through the many thousands of systems available in the AFLOW consortium repository, it is possible to predict a plethora of previously unknown potential quaternary and quinary solid solutions for future experimental validation.

I. INTRODUCTION

High-Entropy Alloys (HEAs) are multi-component alloys forming highly disordered solid solution phases [1–4]. Since their discovery, just over a decade ago, HEAs have attracted the interest of the scientific community, for promising properties and potential applications (see [5–8] as well as Ref. 9 and references therein). The term HEAs, and related terms such as Multiple Principle Element Alloys [3] and Complex Concentrated Alloys [4] often refer to similar alloying concepts. While there may be ongoing discussions in the literature regarding these terms, the approach outlined here is equally applicable to any of these classifications. For the sake of brevity, only the acronym HEAs will be used throughout this article. The ongoing search to discover new high-entropy systems has recently expanded beyond metals to include entropy stabilized ceramics such as high-entropy oxides and carbides [10]. At the time of the discovery, it was conjectured that configurational entropy was the stabilizing mechanism and that many multi-component alloys would form a single phase solid solution. However, further attempts have shown that this is valid only for a fraction of multi-component alloys, while the rest form multiple phases [11]. Therefore, the key factors governing the formation of single phase HEAs remain unknown [12].

Several semi-empirical methods have been proposed to predict which multi-component alloys will form a solid solution (see Ref. 13 for an extensive review). Most approaches use descriptors as screening tools [14–20] with parameters fitted to the available, yet limited, experimental data. Modeling phase diagrams by using CALPHAD has also been applied [3, 21, 22], and it also suffers from insufficient experimental data. Consequently, robust prediction of solid solution forming ability in multi-component alloys remains a major challenge hindering further HEA discovery.

Phase diagram construction of multi-component alloys based on *ab-initio* calculations is a direct method that can compensate for unavailable experimental data (comprehensive review by Widom [23–25]). Computationally very demanding, it involves energy calculations for many configurations and the implementation of statistical mechanical models for estimating thermodynamic properties [26, 27]. Hitherto, it is not surprising that the application of *ab-initio* searches for multi-component alloys has been considered unfeasible and without a predictive role in the search for new HEAs.

Here, a novel high-throughput (HT, [28]) *ab-initio* method is introduced — called LTVC (Lederer-Toher-Vecchio-Curtarolo) — incorporating energy calculations into a mean field statistical mechanics model, and making use of order parameters for predicting the transition temperature of a multi-component system into a solid solution phase. The idea is the following: **i.** The AFLOW [29–36] set of repositories [37–40] for *ab-initio* calculations are leveraged to train cluster expansion (CE) [26, 41] models, within the Alloy Theoretic Automated Toolkit (ATAT) [42] and estimate zero temperature energies of atomic configurations, which are derivative structures of either fcc or bcc lattices, on which HEAs show solid solution forming ability. **ii.** Next, these atomic configurations are incorporated into a mean field statistical mechanical model, named the generalized quasi-chemical approximation (GQCA) [43, 44], which is particularly suitable when long-range order is not important and the material is spatially homogeneous, as expected for solid solutions. **iii.** Finally order parameters are proposed to detect order-disorder phase transitions by following the evolution of the statistical population of ordered configurations.

* stefano@duke.edu

The predictive capability of LTVC is corroborated by Monte Carlo simulations, experimental data for binary alloys [45], CALPHAD calculations performed with Thermo-Calc [46, 47] for ternary alloys, and experimental data of 17 quaternary and quinary alloys shown by experiments to form solid solutions [2, 21, 48–61].

Finally, applying LTVC to quaternary and quinary systems, numerous alloys with solid solution forming ability are identified. These predictions, inaccessible by previously suggested descriptors, show that the method could become an effective guiding tool for HEA design, as well as demonstrate the importance of short-range order in these systems.

II. METHODS

Generation of derivative structures. HEAs form single-phase solid solutions mostly on fcc and bcc lattices [13]: the starting point is the generation of inequivalent atomic decorations of those lattices. A group-theoretical approach [62, 63] is used to generate a complete set of inequivalent atomic configurations with up to 8 atoms and 5 species per primitive cell (Table I), and the multiplicity (degeneracy, number of symmetrically equivalent configurations) of each configuration is calculated. The algorithm is validated with the binary and ternary configurations generated by the `mmaps` code of the ATAT package [64].

at./cell	binary	ternary	quaternary	quinary
2	2	-	-	-
3	6	3	-	-
4	19	39	19	-
5	28	81	108	54
6	80	550	1,360	1,500
7	104	933	3,876	7,600
8	390	6,312	38,372	111,915

TABLE I. Number of inequivalent atomic configurations for fcc and bcc derivative structures including species permutations.

Calculation of zero temperature energies. The AFLOW.org repositories comprise calculated energies of relaxed atomic configurations, which are fcc and bcc derivative structures for most binaries and many ternaries. All *ab-initio* energies are obtained using the VASP software [65] within the AFLOW high-throughput framework [29–36] and using the standardized set of parameters [39]. The vibrational formation enthalpy is usually much smaller than the configurational contribution, especially in highly disordered systems. This allows us to neglect phonon spectra characterization, a daunting challenge for the millions of alloy-structures under investigation [66, 67]. Complete information about these calculations is included in the open access AFLOW.org materials data repository [37–40]. For each alloy system, AFLOW energies are used as input for the `mmaps` code of the ATAT package. Cluster expansion is performed and energies of all configurations with up to 8 atoms per primitive cell are estimated (see binary example in Figure 1(a)). In addition, `mmaps` outputs the cross validation (CV) score, which is a measure for the uncertainty of predicted energies not included in the training set (lower CV score implies less uncertainty). In this article, thermodynamic analysis is performed only for systems whose CV score is less than 50 meV.

Implementation of the GQCA model. The atomic configurations are incorporated into a statistical mechanical mean field model, named the generalized quasi-chemical approximation (GQCA) [43, 44]. This model fits well to high-throughput workflows, as the number of degrees of freedom varies linearly with the number of atomic types in the cell (compared to the cluster variation method [26, 68], whose number of degrees of freedom grows rapidly with cluster size).

The model factorizes a parent lattice of N sites, hosting K species, into non-overlapping space-filling cells of equal number of sites. The clusters are treated as independent, and the total energy of the N-site lattice is approximated as a sum of the n-atom cell energies, each calculated separately. Here, the factorization is implemented using 8-atom cells, and the energy per site of each cell is estimated by assuming periodic boundary conditions on the cell surfaces: each cell has the energy and multiplicity (symmetry degeneracy) of an analog periodic ordering, having 1, 2, 4, or 8 atoms per primitive cell. This implementation suits well the description of ordered or disordered phases having the same parent lattice type, as long as order effects can be captured within 8-atom cells and the spatial homogeneity assumption remains valid (justifying neglect of boundary interactions between phases). In the high-T limit, a fully disordered phase (with ideal entropy of mixing) is represented by cells randomly populating the parent lattice according to the multiplicities. The summation of cell energies over a random distribution to obtain the total energy reduces a potential systematic error, related to the assumption of periodic boundary conditions. In the low-T limit, ordered compounds or elemental phases are trivially demonstrated when only one type of unit cell (periodic ordering) occupies the whole N-site parent lattice. Then, the total energy exactly becomes the sum of the cell's energies. In this article, the GQCA model is implemented only for fcc or bcc type parent lattices. The incorporation of other ordered compounds, not of fcc or bcc type, into the thermodynamic analysis is described below in point **iv** in the section on "Order-disorder transition".

Within the stated assumptions on the GQCA formalism (see Refs. 43 and 44 for details), the thermodynamic potential becomes

$$\Phi = N \cdot \left(\sum\nolimits_j \epsilon_j P_j - Ts - \sum\nolimits_k \mu_k X_k \right), \qquad (1)$$

where $\{P_j\}$ is the probability distribution of finding the

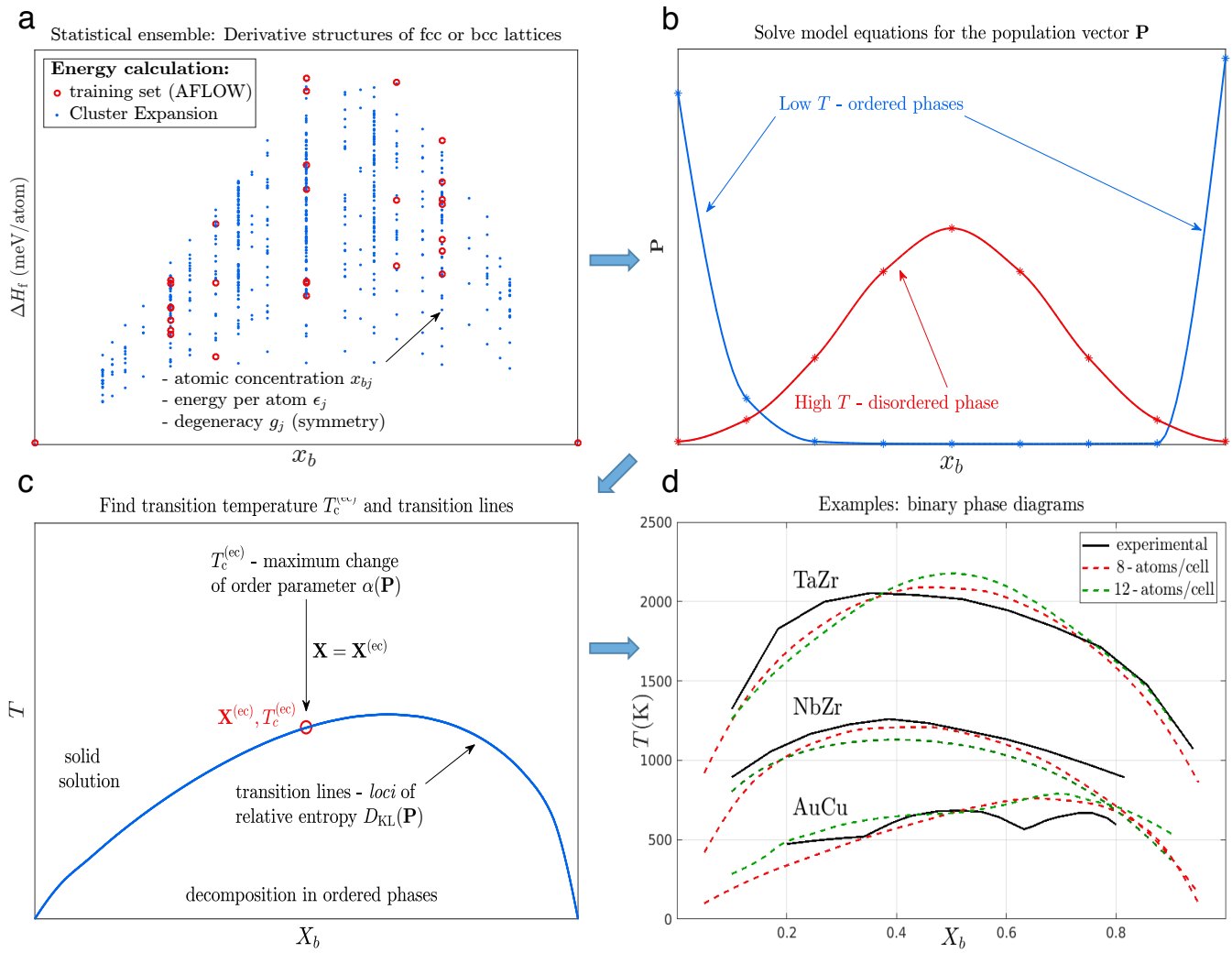

FIG. 1. **Outline of the LTVC method. (a)** Statistical ensemble construction: atomic configurations are generated, multiplicities are calculated, and energies are estimated using cluster expansion trained by the AFLOW dataset. **(b)** The statistical mechanical model is solved for the population vector $\mathbf{P}(\mathbf{X}, T)$ (Eq. (6)). The high-T limit represents a fully disordered phase (Eq. (3)), and the low-T phase separation or ordered compound formation. **(c)** T_c at equi-composition is identified with maximal change of the order parameter α (Eq. (9)). Transition lines are traced as the *loci* of the relative entropy, D_{KL} (Eq. (4)). **(d)** Examples of calculated binary phase diagrams, using a factorization of 8-atom cells (dashed red lines) and 12-atom cells (dashed green lines). Solid black lines represent experimental results, extracted from Ref. [45].

cells with $n = 8$ atoms in the N-site lattice, X_k represents the macroscopic atomic concentration of k-species atoms on the N-site lattice, and ϵ_j, s and μ_k are the energy of j^{th} cell, configurational entropy and the chemical potentials per atom, respectively. The large N limit for the entropy is

$$s = k_B \left(-\sum\nolimits_k X_k \log(X_k) + \frac{1}{n} \sum\nolimits_j P_j \log(P_j/\tilde{P}_j) \right), \tag{2}$$

where k_B is the Boltzmann constant and $\{\tilde{P}_j\}$ is the T-independent random probability distribution of finding the cells in the N-site lattice,

$$\tilde{P}_j = \frac{g_j \prod_k X_k^{n \cdot x_{kj}}}{\sum_{j'} g_{j'} \prod_k X_k^{n \cdot x_{kj'}}}. \tag{3}$$

Here, g_j is the multiplicity of the j^{th} cell and x_{kj} is the fraction of k-species atoms. The first term in Eq. (2) represents the ideal entropy of mixing. The second term,

$$D_{KL}(\mathbf{X}, T) \equiv \frac{1}{n} \sum\nolimits_j P_j \log(P_j/\tilde{P}_j), \tag{4}$$

is known as the relative entropy or the *Kullback-Leibler* divergence [69], and is commonly used to quantify entropy loss due to ordering [70–72]. Minimizing the thermody-

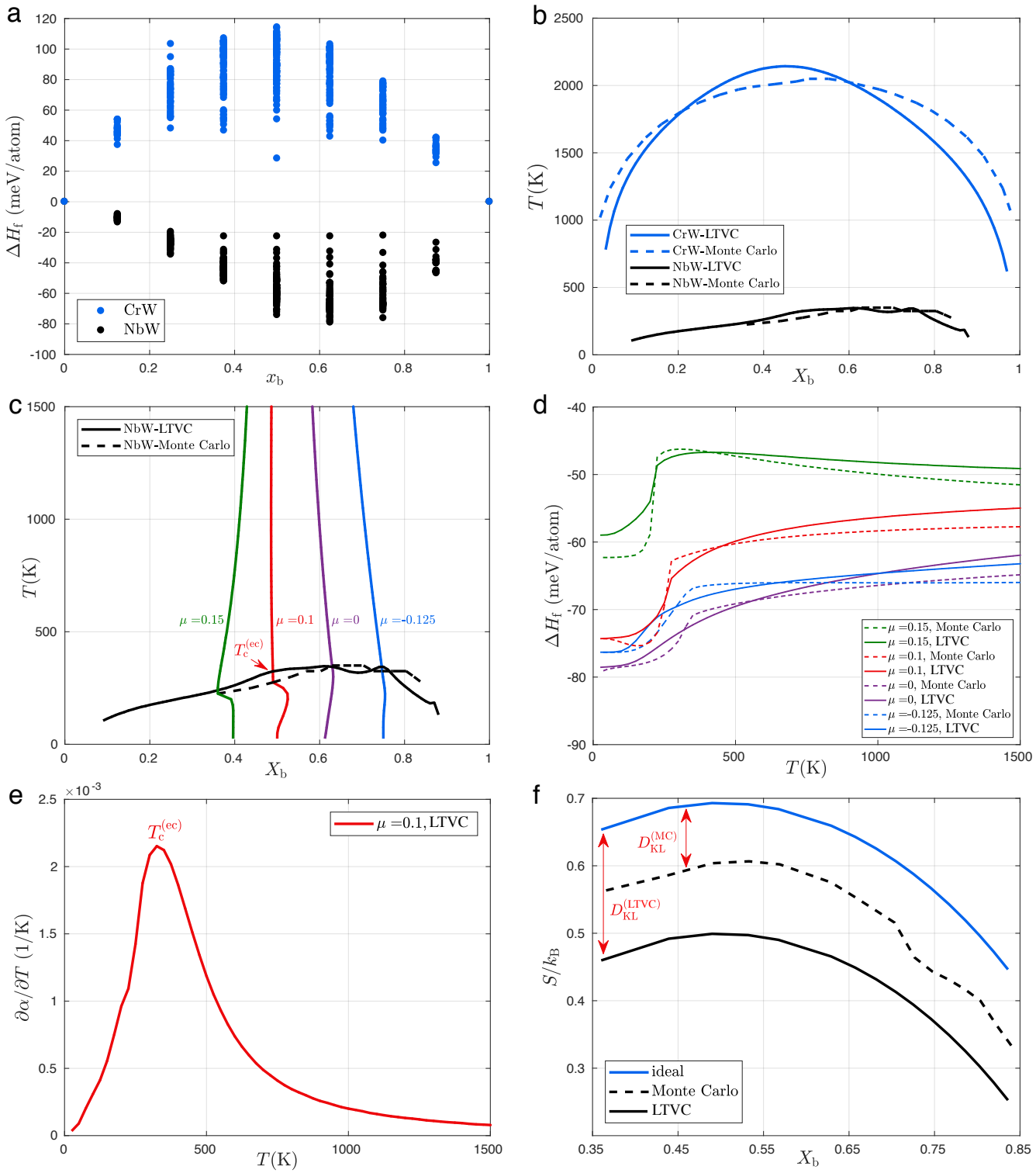

FIG. 2. **Comparison between LTVC and Monte Carlo simulations. (a)** Zero temperature formation enthalpies for CrW (blue) and NbW (black) from cluster expansion, which also drive the Monte Carlo calculations. **(b)** Transition lines for CrW (blue lines) and NbW (black lines), computed using LTVC (solid lines) and Monte Carlo simulations (dashed lines). **(c)** The NbW transition lines, with a sample of constant chemical potential trajectories, taken from the Monte Carlo simulation. **(d)** The NbW formation enthalpies along the $(\mathbf{X}, T)$, constant chemical potential trajectories, computed using LTVC (solid lines) and Monte Carlo simulations (dashed lines). **(e)** Temperature derivative of the order parameter α, Eq. (9), for the NbW case. The equi-composition transition temperature, $T_c^{(ec)}$, is identified as the point where $\partial\alpha/\partial T$ reaches its maximum value. **(f)** Entropy, k_B normalized, across the order-disorder transition lines, computed using LTVC (solid black line) and Monte Carlo simulations (dashed black lines) for the NbW case. The blue line indicates the ideal mixing entropy limit. $D_{KL}^{(model)}$ and $D_{KL}^{(MC)}$ mark the relative entropy reduction, Eq. (4), computed using LTVC and Monte Carlo simulations, respectively. The near constant behavior of $D_{KL}^{(MC)}$ supports the method's assumption.

namic potential, subject to the constraints

$$\sum\nolimits_j P_j = 1; \quad \sum\nolimits_j P_j\, x_{kj} = X_k, \tag{5}$$

the equilibrium probability distribution is found ($\beta = {}^1\!/_{k_{\rm B}T}$):

$$P_j = \frac{\tilde{P}_j\, e^{-n\beta\left(\epsilon_j - \sum_k \mu_k x_{kj}\right)}}{\sum_j \tilde{P}_j\, e^{-n\beta\left(\epsilon_j - \sum_k \mu_k x_{kj}\right)}}. \tag{6}$$

The expression for the probability distribution is reinserted into Eq. (5) for the $(K-1)$ independent $\mu_k(\mathbf{X},T)$ functions of temperature and macroscopic concentration[1]. The thermodynamic potential, Eq. (1), and its related thermodynamic quantities are then easily obtained as functions of temperature and macroscopic concentration.

Order-disorder transition. The random population vector $\tilde{\mathbf{P}}$, Eq. (3), is the high-T limit of population vector $\mathbf{P}$, Eq. (6). The limit represents a fully disordered phase with ideal entropy of mixing (only the first term in Eq. (2) being non-zero, while the relative entropy vanishes). An order-disorder transition *locus*, $\tilde{T}_{\rm c}(\mathbf{X})$, can be found as the intersection between the potential of a fully disordered phase

$$\tilde{\Phi}_{\rm disorder}(\mathbf{X},T) \equiv \lim_{\mathbf{P}\to\tilde{\mathbf{P}}} \Phi(\mathbf{X},T), \tag{7}$$

with that of a competing ordered phase, $\Phi^{\rm AFLOW}_{\rm order}(\mathbf{X})$, estimated by using the AFLOW convex-hull database [73],

$$\tilde{\Phi}_{\rm disorder}(\mathbf{X},\tilde{T}_{\rm c}) = \Phi^{\rm AFLOW}_{\rm order}(\mathbf{X}) \Rightarrow \tilde{T}_{\rm c}(\mathbf{X}). \tag{8}$$

The approach, equivalent to a common-tangent construction of the two asymptotic free energies, is straightforward. Unfortunately, it disregards the effect of short range order on both the energy and entropy of the disordered phase, potentially leading to erroneous transition temperatures.

To overcome this issue, a two-step algorithm (marked **i-ii**) is proposed. In spirit, it is similar to what is done for phase-diagram construction using Monte-Carlo simulations, where an order parameter locating an order-disorder transition is followed by an algorithm tracing the boundary line.

i. *Estimation of the order-disorder transition temperature at equi-composition.* The change of the population vector from the high-T limit (representing full disorder), to the low-T limit (representing ordered compounds or elemental phases), motivates the introduction of the order parameter:

$$\alpha\,(\mathbf{X},T) \equiv \mathbf{P}\cdot\tilde{\mathbf{P}}/|\mathbf{P}||\tilde{\mathbf{P}}|, \tag{9}$$

which measures the deviation of the population vector from the high-T limit. Similar to the behavior of the order parameter in Monte-Carlo simulations [27], maximal change is expected at order-disorder transition (see Figure 2(e)). The transition temperature at equi-composition $T_{\rm c}^{\rm (ec)}$ is identified as the point where $\partial\alpha/\partial T$ reaches its maximum value (red circle in Figure 1(c)).

ii. *Tracing the boundary lines.* Near the solid solution boundary lines, the entropy of the disordered phase decreases due to the growth of short range order. The boundary lines separating solid solutions and decomposition into ordered phases (blue line in Figure 1(c)) are found, assuming entropy reduction is approximately constant across them

$$D_{\rm KL}(\mathbf{X},T_{\rm c}) \approx D_{\rm KL}(\mathbf{X}^{\rm (ec)},T_{\rm c}^{\rm (ec)}). \tag{10}$$

Here, $D_{\rm KL}$ is the relative entropy, defined in Eq. (4), $T_{\rm c}^{\rm (ec)}$ is the transition temperature at equi-concentration, $\mathbf{X}^{\rm (ec)}$, and $T_{\rm c}$ is the transition temperature at $\mathbf{X}$. The approximation works well for alloys characterized by relatively simple phase diagrams (see Figure 2(f)). For more complex systems, involving the formation of multiple ordered phases at low temperatures (as predicted by the AFLOW convex hull), a more accurate method should involve a detailed study of the population vector $\mathbf{P}(\mathbf{X},T)$ at low temperatures. Since HEAs usually form near equi-composition, step **ii** is not critical, and the results reported are based on the use of only α as the order parameter.

iii. *Predicting the solid solution parent lattice.* Steps **i-ii** are independently implemented for fcc and bcc lattices. The lowest thermodynamic potential, Eq. (1), will determine the structure of the solid solution.

iv. *Effect of other competing ordered phases.* The formation of ordered phases, not of fcc or bcc type, might raise the order-disorder transition temperature in some parts of the phase diagram. Using the AFLOW convex-hull, the minimal thermodynamic potential of all other ordered phases $\Phi^{\rm AFLOW}_{\rm order}(\mathbf{X})$ is estimated, leading to a potentially higher transition temperature:

$$\Phi(\mathbf{X},T^{\rm gs}_{\rm c}) = \Phi^{\rm AFLOW}_{\rm order}(\mathbf{X}) \Rightarrow T^{\rm gs}_{\rm c}(\mathbf{X}). \tag{11}$$

If $T^{\rm gs}_{\rm c}$ is higher than $T_{\rm c}$ found by steps **i-ii-iii**, then $T^{\rm gs}_{\rm c}$ is used as a better estimate for the transition temperature $T_{\rm c}$.

Test of cell size factorization convergence. Figure 1(d) compares calculated with experimental boundary lines, taken from Massalski *et al.* [45]. To test LTVC's convergence with respect to cell size, calculations are performed using 8-atom cells and 12-atom cells (dashed red and green lines, respectively). Similarity between calculated and experimental boundaries demonstrates the method's ability to follow order-disorder transitions at equi-composition when either phase separation (NbZr and TaZr) or ordered compound formation (AuCu) oc-

[1] vector $\mathbf{X}$ represents the macroscopic concentrations X_k.

cur at low temperatures.

Comparison of the LTVC method *versus* Monte Carlo simulations. Monte Carlo (MC) simulations are accurate — albeit computationally demanding — tools for calculating thermodynamic properties. LTVC and MC results are compared. The latter are obtained with the `ATAT-memc2` code [27]. Comparisons provide direct and reliable benchmarks as the two approaches are driven by the same cluster expansion. Two representative alloys were chosen: CrW and NbW. Figure 2(a) shows the zero temperature formation enthalpies of CrW (blue) and NbW (black), as obtained from a cluster expansion on a bcc parent lattice. The two alloys exhibit very different energy landscapes. The positive formation enthalpies of CrW leads to phase separation to elemental phases at low temperatures, while the negative formation enthalpies of NbW promote ordered compounds.

Figure 2(b) shows the order-disorder transition lines of the two alloys, using LTVC (solid lines) and MC (dashed lines). For a wide concentration range, the agreement demonstrates the ability of the method to accurately reproduce order-disorder transitions when ordered compound formation or phase separation appear at low temperature.

Figures 2(c-f) depicts the NbW case. Panel (c) shows a sample of constant chemical potential trajectories, obtained from the MC simulations. Panel (d) compares the formation enthalpy along such (X, T) trajectories, using LTVC (solid lines) and MC simulations (dashed lines). The agreement demonstrates the ability of the method to accurately estimate the Gibbs free energy of the alloy both at high (disorder) and low temperatures (order).

Figure 2(e) shows the temperature derivative of the order parameter α (Eq. (9)) along the equi-composition trajectory ($\mu = 0.1$ red line in Figure 2(c)). The sensitivity of α to the underlying phase transition allows easy identification of $T_c^{(ec)} = 325$K, close to the MC prediction (275K). Panel (f) depicts the entropy estimated by LTVC and the MC simulations along their respective boundary lines. First, despite $D_{KL}^{(MC)}$ — the entropy reduction from the ideal mixing entropy limit (blue line) — being smaller than $D_{KL}^{(model)}$, Eq. (4), the model predictions do not depend on the absolute value of D_{KL} at $T_c^{(ec)}$, so the difference is irrelevant. Second, the small variation of $D_{KL}^{(MC)}$ justifies the working assumption about the transition lines as the *loci* of relative entropy, Eq. (10). In conclusion, LTVC's combination of order parameter α and the relative entropy D_{KL} leads to boundaries very similar to those obtained from MC.

III. RESULTS

Binary alloys. The experimental data for 117 binary alloys is collected [45] and compared with the predictions. For each system, cluster expansion is performed separately on bcc and fcc lattices. The energies of all inequivalent atomic configurations with up to 8 atoms per primitive cell (631 for each lattice) are estimated. Thermodynamic analysis is then performed as described above and the transition temperature T_c at equi-composition is estimated. The standard deviation of T_c is estimated as follows: zero temperature energies, predicted by cluster expansion, are randomly shifted according to a normal distribution. The standard deviation of the normal distribution is the CV score, retrieved from the output of the `mmaps` code of ATAT. Thermodynamic analysis is performed repeatedly, each time with new shifted energies, until convergence of the standard deviation of T_c is obtained. A solid solution is predicted if $T_c < T_m^{(exp)}$, where $T_m^{(exp)}$ is the experimental melting temperature at the appropriate composition. The results are presented in Figure 3 and listed in Table III.

- *Existence.* Formation (or not) of the solid solution is correctly reproduced in 102 out of 117 analyzed systems with an effectiveness of $\eta_{ss} = 102/117 = 87.2\%$.
- *Solid solution forming systems.* 56 out of the 58 predicted solid solution-forming are experimentally corroborated with correct underlying lattice: $\eta_{latt} = 56/58 = 96.6\%$. In such cases, LTVC tends to overestimate the transition temperature by ∼11%.
- *Non solid solution forming systems.* 46 out of 59 systems predicted not to form a solid solution phase are experimentally verified as such. Erroneous prediction of 9 out of 13 alloys is explained by the estimated standard deviation of T_c.
- Three binaries (AuNi, MnNi, MnV) exhibit differences greater than 3 standard deviations between calculated and experimental transition temperatures. Test Monte Carlo simulations, performed using ATAT [27], predict T_c values similar to those of LTVC. Likely, the problem is related to the neglect of vibrational formation entropy coming from phonon contributions (AuNi, one of these three alloys, is known to have large vibrational entropy of formation [74]), or to insufficient training data: the zero temperature formation enthalpy calculations (performed on primitive cells with 4 atoms or less) could be incommensurate with larger-size order effects (*e.g.* magnetic), and thus effectively overestimate the transition temperatures.
- The two approaches $\tilde{T}_c$, Eq. (8), and T_c, steps **i-iv**, produce similar results, indicating that for binaries the effect of short range order is limited. Later, we will show that this will not be the case for ternaries.

Ternary alloys. Next, the complete set of 4,495 ternary alloys that can be formed from 31 species is addressed[2]. In the absence of an extensive database of experimentally studied ternary alloys, the predictions of the LTVC

[2] Ag, Al, As, Au, Co, Cr, Cu, Fe, Ge, Hf, Ir, Mn, Mo, Nb, Ni, Os, Pd, Pt, Re, Rh, Ru,Sb, Sc, Si, Ta, Tc, Ti, V, W, Y, and Zr.

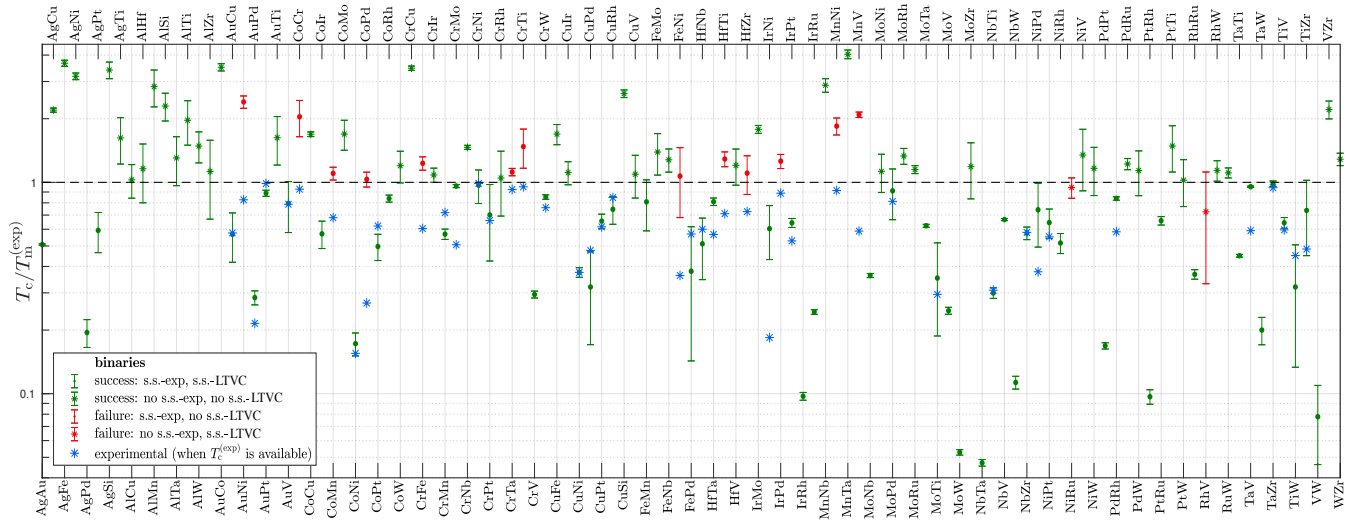

FIG. 3. $T_c/T_m^{(exp)}$ and success rate for 117 binary alloys (alphabetic order). A solid solution is predicted by LTVC if $T_c < T_m^{(exp)}$ (points below the dashed line). Success rate of 87.2% is calculated as ratio of successes (in green) to total [successes+failures]; (failures in red).

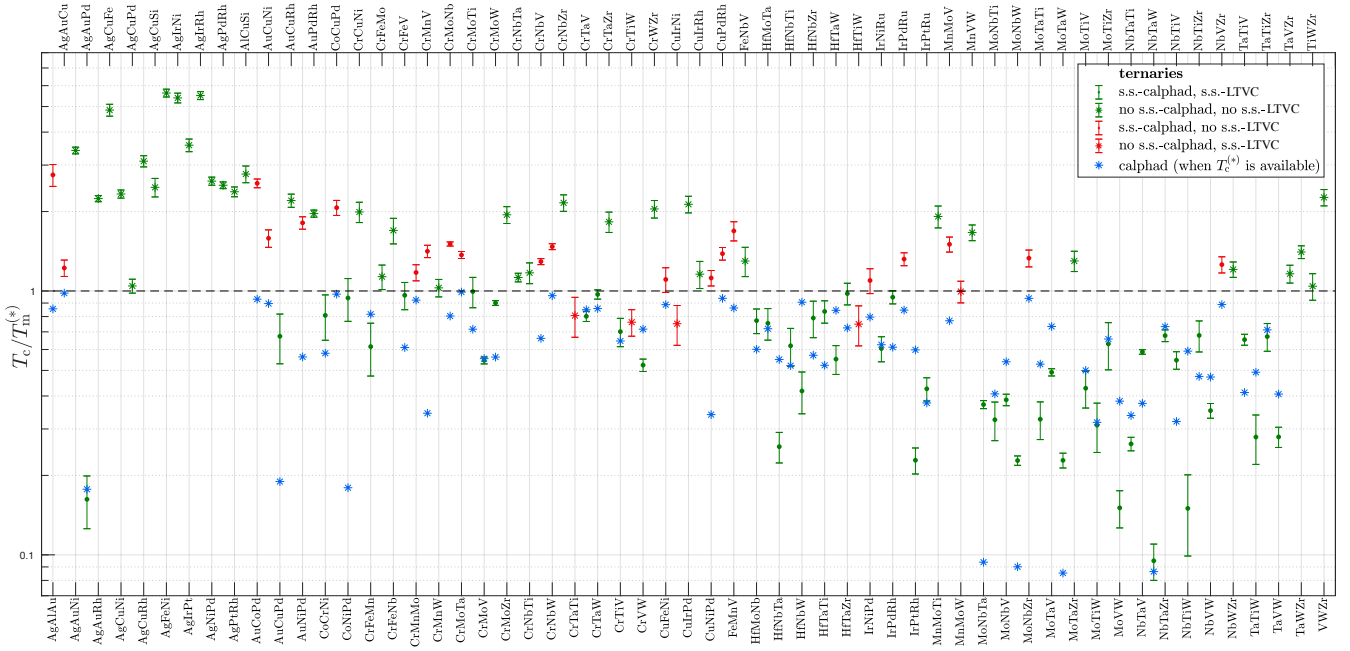

FIG. 4. $T_c/T_m^{(*)}$ and comparison with CALPHAD predictions for 113 ternary alloys (alphabetic order). $T_m^{(*)}$ is the solidus temperature taken from CALPHAD. A solid solution is predicted by LTVC if $T_c < T_m^{(*)}$ (points below the dashed line). Success rate of 77.0% is calculated as ratio of successes (in green) to total [successes+failures]; (failures in red).

method are compared with the results of calculations employing the CALPHAD methodology [3, 21, 22].

i. *CALPHAD.* Phase diagram calculations are performed using the Thermo-Calc software and the SSOL5 database for binary and ternary alloys [46, 47]. The following parameters are assessed at equi-composition: the *solidus* temperature, $T_m^{(*)}$, the number and types of phases at this temperature, the first reaction temperature below $T_m^{(*)}$ and the number and types of phases below the first reaction temperature. Formation (or not) of a solid solution is then tested, along with its underlying lattice and the critical temperature, $T_c^{(*)}$. Although these predictions are based mainly on extrapolation of binary data, they are expected to be reasonably reliable, as long as the associated binaries of each ternary alloy are included in the SSOL5 database. Cases where the solid solution phase found by Thermo-Calc is of hcp type are not included in the comparison (as *ab-initio* modeling of a solid

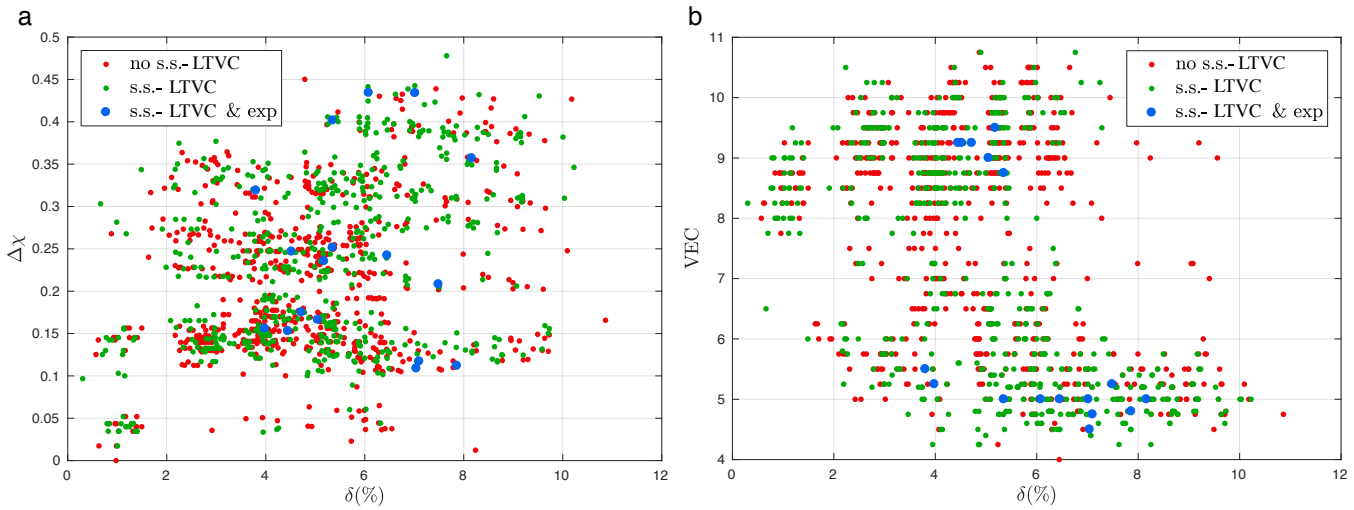

FIG. 5. The failure of empirical parameters, suggested as descriptors for HEAs, to pinpoint solid solutions. Model predictions for quaternary and quinary alloys (green - predicted s.s., blue - predicted s.s. and verified by experiments, see Table II) are plotted as a function of: **(a)** the electro-negativity difference ($\Delta\chi$) [15] and the atomic size difference (δ) [14]; **(b)** the valence electron concentration (VEC) [19] and the atomic size difference (δ).

solution phase was not performed on this lattice).

ii. *Ab-initio method.* As for binaries, cluster expansion is performed for each ternary alloy on bcc and fcc lattices using the available training data of the AFLOW repositories. Cluster expansion is performed and the energies of all inequivalent configurations (9,808 for each lattice) are estimated. Thermodynamic analysis is performed for ternaries whose CV score is less than 50 meV and their transition temperature T_c at equi-composition is obtained, along with its estimated standard deviation. A solid solution is predicted if $T_c < T_m^{(\star)}$.

Results of *ab-initio* and CALPHAD for 441 ternaries are listed in Table IV. Figure 4 shows the results for 113 ternaries whose CV score is less than 30 meV and the 3 associated binaries of each ternary alloy are found in the SSOL5 database.

- *Existence.* Formation (or not) of the solid solution is in agreement for 87 out of 113 ternaries with an effectiveness of $\eta_{ss} = 87/113 = 77.0\%$.
- *Solid solution forming systems.* 49 out of the 54 predicted solid solution-forming cases are corroborated by CALPHAD with correct underlying lattice: $\eta_{latt} = 49/54 = 90.7\%$. The transition temperatures of these 49 ternaries are in good agreement. In such cases, the method predicts transition temperatures slightly higher (∼3%) than CALPHAD. Formation of solid solutions is not corroborated by CALPHAD in 5 out of 54 cases. Here, the disagreement between the two methods can be related to the standard deviation of T_c as well. Note that for 4 of these 5 cases, CALPHAD exhibits the same solid solution phase below $T_m^{(*)}$, accompanied by an additional phase.
- *Non solid solution forming systems.* 38 out of 59 non-forming predicted cases are corroborated by CALPHAD. Out of the 21 cases in disagreement, 15 are not explained by the standard deviations of T_c (differences are of greater than 3 standard deviations). As for binaries, the problem could be related to the fact that the LTVC method neglects the vibrational entropy of formation, or to insufficient training data for cluster expansion calculations.
- $\tilde{T}_c$ values (approximated according to Eq. (8)) are lower than T_c by 38.3% and 20 of its 86 predicted solid solution-forming cases are in disagreement with CALPHAD. This shows that the effect of short range order on transition temperature is non-negligible for ternaries.

Search for quaternary and quinary HEAs. As before, for each alloy, cluster expansion is performed separately on bcc and fcc lattices, based on the available training data of the AFLOW repositories. The energies of all inequivalent configurations (79,185 for quaternaries, 425,219 for quinaries) are estimated. Thermodynamic analysis is performed for alloys whose CV score is less than 50 meV, and the transition temperature T_c at equi-composition is obtained. The results for 1110 quaternary alloys and 130 quinary alloys (mainly those based on the refractory elements Cr, Hf, Mo, Nb, Ta, Ti, V, W and Zr) are listed in Tables V and VI, respectively. 571 of the 1240 quaternaries and quinaries show solid solution forming ability. These numbers demonstrate that among multi-component alloys, one can expect to find a plethora of solid solutions. Table II shows results for alloys, demonstrated by experiments to form solid solutions [2, 21, 48–61]. The data of all experimentally studied alloys and T_c values of Monte-Carlo simulations [23, 24] corroborates the method's accuracy. $\tilde{T}_c$ values (approximated according to Eq. (8)) are significantly lower, demonstrating again the importance of short range order effects.

As mentioned, several empirical parameters have been

TABLE II. Comparison between LTVC and experimental data for quaternaries and quinaries. S.S. type of single phase solid solution; T_c (K) calculated transition temperature; $\tilde{T}_c$ (K) approximated transition temperature, estimated according to Eq. (8); $\bar{T}_m$ (K) melting temperature (solidus), calculated as the average of the melting temperatures at equi-composition of the binaries associated with the alloy; A solid solution is predicted if $T_c < \bar{T}_m$; CV (meV) cluster expansion cross validation score; S.S. Exp. type of single phase solid solution found in experiments.

HEA	S.S.	T_c	$\tilde{T}_c$	$\bar{T}_m$	CV	S.S. Exp.
CoCrFeNi	fcc	1,600	1,000	1,720 [a]	47	fcc [48, 49]
CoCrMnNi	fcc	1,280	1,020	1,580	37	fcc [48]
CoFeMnNi	fcc	1,550	900	1,600	48	fcc [21, 48]
AlNbTiV	bcc	1,260	1,070	1,975	50	bcc [51]
HfNbTiZr	bcc	970	840	2,135	22	bcc [52]
MoNbTaW	bcc	1,010 [b]	540	3,065	4	bcc [53, 54]
NbTaTiV	bcc	970	800	2,345	6	bcc [55]
NbTiVZr	bcc	1,400 [c]	1,110	1,955	16	bcc [56]
CoCrFeMnNi	fcc	850	950	1,640	43	fcc [2]
AlCrMoTiW	bcc	1,650	1,000	2,150	44	bcc [58]
HfNbTaTiZr	bcc	1,300	750	2,280	17	bcc [59]
HfNbTiVZr	bcc	1,750	900	2,020	21	bcc [61]
MoNbReTaW	bcc	2,750	1,100	3,000	14	bcc [60]
MoNbTaTiV	bcc	800	450	2,470	8	[60]
MoNbTaVW	bcc	1,000	500	2,800	5	bcc [53, 54]
MoNbTiVZr	bcc	1,450	700	2,120 [d]	17	bcc [57]
NbReTaTiV	bcc	950	800	2,470	19	bcc [60]

[a] $T_m^{(exp)}$=1,695K [48]
[b] Monte Carlo predicts T_c =1,280K [24]
[c] Monte Carlo predicts T_c =1,250K [23]
[d] $T_m^{(exp)}$=2,380K [57]

proposed as descriptors for single phase HEAs. Until now, they were only tested versus very limited experimental data. The new predictions serve as a much larger test set. Figure 5 shows that three of the suggested descriptors: the electro-negativity difference ($\Delta\chi$) [15], the atomic size difference (δ) [14] and the valence electron concentration (VEC) [19] (see [11] for formulas and values used in this article for these parameters), fail to pinpoint the quaternary and quinary solid solutions predicted by LTVC. Although not presented here, it is noted that another descriptor, based on enthalpies of formation calculated for binary compounds [20], also fails to identify the alloys forming solid solutions according to LTVC. These findings challenge the view that these simple descriptors can serve as an effective search tool for single phase HEAs.

IV. CONCLUSIONS

Robust prediction of solid solution forming ability in multi-component alloys remains a major challenge hindering the discovery of novel HEAs. This article introduces a novel high-throughput method — called LTVC — enabling *ab-initio* searches through the vast space of possible multi-component alloys of solid solutions. Based on the synergy of AFLOW repositories, cluster expansion and a straightforward, yet accurate, mean field theory model, the approach can become an effective and efficient guiding tool for HEA design.

The accuracy is corroborated by Monte Carlo simulations, experimental data for binaries (87.2% agreement), CALPHAD calculations for ternaries (77.0% agr.) and experimental data for 17 quaternary and quinary alloys (100% agr.). Solid solution-forming cases are confirmed with high success rate: 96.6%, 90.7%, 100% and 100% for binaries, ternaries quaternaries and quinaries, respectively. The underlying lattice of the solid solution is correctly predicted as well. Transition temperatures, when available from experiments or CALPHAD predictions, are also in good agreement: LTVC predicts transition temperatures slightly higher than the experimental values for binaries (∼11%) and CALPHAD values for ternaries (∼3%).

Cases in disagreement with experiments or CALPHAD, when found, are likely related to the neglect of vibrational formation entropy or to insufficient training data for cluster expansion, pointing to future directions for improvement of the method. The presented results identify potential stable solid solution candidates. Often, sluggish kinetics is the bottleneck in achieving equilibrium, so many transition temperatures might be quite difficult to characterize experimentally.

Analysis of 1110 quaternary and 130 quinary alloys show that 46% of them form solid solutions, suggesting that there are ample single phase HEAs yet to be discovered. *Ab-initio* modeling of hcp solid solution phases has not been performed yet, a future avenue of investigation for the model. Furthermore, the extension to non-equiatomic alloys still remains a daunting task without more information on concentration ranges.

It is proved that short range order effects are also crucial for correct solid solution-forming predictions: other methods, neglecting such effects on configurational entropy, are likely to significantly underestimate the transition temperature to a solid solution phase — possible erroneous prediction of solid solution-formation. Finally, previously suggested descriptors [14, 15, 19, 20] did not produce many of the solid solutions predicted here, casting doubts on the capability of such descriptors to serve as effective searching tools. The directions suggested in this article will facilitate the critical work of acquisition of new experimental data.

ACKNOWLEDGMENTS

We thank Ohad Levy, Donald Brenner, Jon-Paul Maria, Corey Oses, Matthias Scheffler, and Luca Ghiringhelli for various technical discussions. We acknowledge support by DOD-ONR (N00014-13-1-0635, N00014-11-1-

0136, N00014-15-1-2863). S.C. acknowledges the Alexander von Humboldt Foundation for financial support. The consortium AFLOW.org acknowledges Duke University – Center for Materials Genomics — for computational support.

A. Binary alloys at equi-composition

TABLE III: LTVC results for binary alloys. S.S. type of single solid solution phase ("none" = not found); T_c (K) transition temperature, as estimated by the method; $\tilde{T}_c$ (K) approximated transition temperature, estimated according to Eq. (8); CV (meV) cluster expansion cross validation score; S.S. Exp. type of single solid solution phase found experimentally ("none" = not found); $T_c^{(exp)}$ (K) experimental transition temperature; $T_m^{(exp)}$ (K) experimental melting temperature (*solidus*).

	S.S.	T_c	$\tilde{T}_c$	CV	S.S. Exp.	$T_c^{(exp)}$	$T_m^{(exp)}$		S.S.	T_c	$\tilde{T}_c$	CV	S.S. Exp.	$T_c^{(exp)}$	$T_m^{(exp)}$
AgAu	fcc	660	750	1	fcc		1,300	AgCu	none	2,350	1,450	8	none		1,070
AgFe	none	6,590	5,400	22	none		1,800	AgNi	none	5,620	3,480	21	none		1,770
AgPd	fcc	300	310	7	fcc		1,540	AgPt	fcc	1,090	650	23	fcc		1,840
AgSi	none	5,270	5,390	36	none		1,550	AgTi	none	2,790	3,050	45	none		1,720
AlCu	none	1,130	1,480	21	none		1,100	AlHf	none	2,400	3,790	47	none		2,070
AlMn	none	4,170	2,750	50	none		1,470	AlSi	none	3,030	4,280	35	none		1,320
AlTa	none	2,960	2,540	48	none		2,270	AlTi	none	3,480	2,850	50	none		1,770
AlW	none	2,850	3,390	36	none		1,920	AlZr	none	1,970	3,870	49	none		1,750
AuCo	none	5,150	3,420	21	none		1,470	AuCu	fcc	670	680	19	fcc	680	1,180
AuNi	none	3,050	1,820	21	fcc	1,050	1,270	AuPd	fcc	490	630	6	fcc	370	1,720
AuPt	fcc	1,350	810	7	fcc	1,500	1,520	AuTi	none	2,880	2,820	47	none		1,770
AuV	fcc	1,310	1,850	30	fcc	1,300	1,650	CoCr	none	3,410	2,270	44	bcc	1,550	1,670
CoCu	none	2,820	1,910	10	none		1,670	CoIr	fcc	1,010	630	17	fcc		1,770
CoMn	none	1,620	1,600	14	fcc	1,000	1,470	CoMo	none	3,080	3,470	37	none		1,820
CoNi	fcc	300	320	6	fcc	270	1,740	CoPd	none	1,540	1,000	15	fcc	400	1,490
CoPt	fcc	880	920	15	fcc	1,100	1,770	CoRh	fcc	1,400	1,010	8	fcc		1,670
CoW	none	3,320	4,080	40	none		2,770	CrCu	none	6,310	4,260	17	none		1,820
CrFe	none	2,240	1,300	18	bcc	1,100	1,820	CrIr	none	2,460	3,210	20	none		2,270
CrMn	bcc	950	970	8	bcc	1,200	1,670	CrMo	bcc	2,180	1,320	6	bcc	1,150	2,270
CrNb	none	2,810	2,380	9	none		1,920	CrNi	fcc	1,570	1,920	26	fcc	1,600	1,620
CrPt	fcc	1,380	2,400	39	fcc	1,300	1,970	CrRh	none	1,960	2,310	44	none		1,870
CrTa	none	2,540	3,010	13	bcc	2,100	2,270	CrTi	none	2,480	2,770	38	bcc	1,600	1,680
CrV	bcc	610	540	4	bcc		2,070	CrW	bcc	2,190	1,360	8	bcc	1,950	2,570
CuFe	none	2,910	2,300	28	none		1,720	CuIr	none	2,270	1,740	26	none		2,040
CuNi	fcc	570	360	5	fcc	570	1,520	CuPd	fcc	470	770	22	fcc	700	1,470
CuPt	fcc	1,160	1,060	12	fcc	1,090	1,770	CuRh	fcc	1,170	880	19	fcc	1,330	1,570
CuSi	none	3,600	3,770	17	none		1,370	CuV	none	2,480	2,250	40	none		2,270
FeMn	fcc	1,310	1,440	30	fcc		1,620	FeMo	none	2,880	2,020	43	none		2,070
FeNb	none	2,390	2,770	27	none		1,870	FeNi	none	1,830	1,100	44	bcc	620	1,710
FePd	fcc	600	1,070	31	fcc	900	1,580	HfNb	bcc	1,280	1,410	33	bcc	1,500	2,500
HfTa	bcc	2,000	2,110	11	bcc	1,400	2,470	HfTi	none	2,540	2,190	21	bcc	1,400	1,970
HfV	none	2,130	2,950	33	none		1,770	HfZr	none	2,510	2,180	38	bcc	1,650	2,270
IrMo	none	4,400	3,760	20	none		2,470	IrNi	fcc	1,310	1,010	31	fcc	400	2,170
IrPd	none	2,480	1,730	20	fcc	1,750	1,970	IrPt	fcc	1,460	990	10	fcc	1,200	2,270
IrRh	fcc	250	220	2	fcc		2,570	IrRu	fcc	650	780	3	fcc		2,670
MnNb	none	4,810	3,380	30	none		1,670	MnNi	none	2,380	1,980	22	fcc	1,180	1,290
MnTa	none	6,740	4,710	28	none		1,670	MnV	none	3,800	2,970	14	bcc	1,070	1,820
MoNb	bcc	1,040	900	4	bcc		2,870	MoNi	none	2,220	2,860	35	none		1,970
MoPd	fcc	1,850	2,180	37	fcc	1,650	2,030	MoRh	none	3,090	2,710	25	none		2,320

	S.S.	T_c	$\tilde{T}_c$	CV	S.S. Exp.	$T_c^{(exp)}$	$T_m^{(exp)}$		S.S.	T_c	$\tilde{T}_c$	CV	S.S. Exp.	$T_c^{(exp)}$	$T_m^{(exp)}$
MoRu	none	2,610	2,910	14	none		2,270	MoTa	bcc	1,850	1,560	5	bcc		2,970
MoTi	bcc	800	1,170	31	bcc	670	2,270	MoV	bcc	610	630	4	bcc		2,470
MoW	bcc	170	180	1	bcc		3,220	MoZr	none	2,160	2,660	43	none		1,820
NbTa	bcc	140	130	1	bcc		2,970	NbTi	bcc	650	760	6	bcc	670	2,170
NbV	bcc	1,480	1,630	3	bcc		2,220	NbW	bcc	330	400	4	bcc		2,920
NbZr	bcc	1,190	1,420	11	bcc	1,200	2,070	NiPd	bcc	1,120	700	31	bcc	570	1,510
NiPt	fcc	1,110	880	19	fcc	950	1,720	NiRh	fcc	940	660	13	fcc		1,820
NiRu	fcc	1,720	1,910	20	none		1,820	NiV	none	1,980	2,330	43	none		1,470
NiW	none	3,110	3,690	49	none		2,670	PdPt	fcc	310	270	2	fcc		1,840
PdRh	fcc	1,610	1,060	5	fcc	1,120	1,920	PdRu	none	2,260	2,590	16	none		1,850
PdW	none	2,370	2,890	40	none		2,085	PtRh	fcc	210	240	3	fcc		2,170
PtRu	fcc	1,560	1,480	10	fcc		2,370	PtTi	none	3,120	4,700	48	none		2,100
PtW	none	2,560	2,970	43	none		2,500	RhRu	fcc	870	900	7	fcc		2,370
RhV	fcc	1,320	2,650	46	none		1,820	RhW	none	2,870	2,900	28	none		2,520
RuW	none	2,740	3,140	17	none		2,470	TaTi	bcc	1,110	1,150	3	bcc		2,470
TaV	bcc	2,260	2,360	3	bcc	1,400	2,370	TaW	bcc	690	640	13	bcc		3,450
TaZr	bcc	2,090	2,070	9	bcc	2,000	2,120	TiV	bcc	1,210	1,390	10	bcc	1,120	1,880
TiW	bcc	710	890	33	bcc	1,000	2,220	TiZr	bcc	1,340	1,600	38	bcc	880	1,820
VW	bcc	200	360	11	bcc		2,570	VZr	none	3,470	3,050	29	none		1,570
WZr	none	3,950	4,170	25	none		3,070								

B. Ternary alloys at equi-composition

TABLE IV: LTVC results for ternary alloys. S.S. type of single solid solution phase ("none" = not found); T_c (K) transition temperature, as estimated by the method; $\tilde{T}_c$ (K) approximated transition temperature, estimated according to Eq. (8); CV (meV) cluster expansion cross validation score; S.S.$^{(\star)}$ type of single solid solution phase using CALPHAD ("none" = not found); $T_c^{(\star)}$ (K) transition temperature, as estimated by CALPHAD; $T_m^{(\star)}$ (K) melting temperature (solidus), as estimated by CALPHAD; $n^{(\star)}$ number of binary alloys (3 possible for each ternary) found in the SSOL5 database of Thermo-Calc.

	S.S.	T_c	$\tilde{T}_c$	CV	S.S.$^{(\star)}$	$T_c^{(\star)}$	$T_m^{(\star)}$	$n^{(\star)}$		S.S.	T_c	$\tilde{T}_c$	CV	S.S.$^{(\star)}$	$T_c^{(\star)}$	$T_m^{(\star)}$	$n^{(\star)}$
AgAlAu	none	2,670	2,530	27	fcc	830	970	3	AgAlFe	none	7,000	7,000	38	none		1,050	3
AgAlNi	none	6,020	3,690	37	none		1,220	3	AgAlV	none	5,160	2,650	45	none		1,040	3
AgAsAu	none	2,780	1,820	36	none		900	2	AgAsCu	none	1,920	1,780	27	none		800	1
AgAsPd	none	1,660	1,620	37	none		1,010	1	AgAuCo	none	4,880	2,920	35	none		1,310	2
AgAuCu	none	1,320	720	10	fcc	1,060	1,080	3	AgAuFe	none	6,490	2,680	41	none		1,280	2
AgAuMo	none	4,200	3,870	39	none		1,280	2	AgAuNi	none	4,840	1,850	15	none		1,420	3
AgAuPd	fcc	250	390	6	fcc	273	1,540	3	AgAuPt	fcc	1,110	560	7	fcc	1,070	1,450	2
AgAuRh	none	4,860	1,970	14	none		2,170	3	AgAuSi	none	3,100	2,450	39	none		920	3
AgAuTi	none	2,350	1,830	38	none		1,230	3	AgAuV	none	4,630	2,340	38	none		1,290	2
AgCoCu	none	5,440	2,570	22	none		1,250	2	AgCoPd	none	5,230	2,040	21	fcc	650	1,500	2
AgCoPt	none	5,020	2,090	30	none		1,370	2	AgCoRh	none	6,390	2,670	24	none		1,370	1
AgCuFe	none	5,090	2,560	28	none		1,050	3	AgCuIr	none	4,940	2,440	32	none		1,050	3
AgCuMn	none	5,260	2,200	48	none		1,060	3	AgCuNi	none	3,730	1,520	14	none		1,600	3
AgCuPd	none	1,400	800	9	none		1,340	3	AgCuPt	none	1,970	1,160	12	none		1,190	2
AgCuRh	none	3,290	1,540	17	none		1,060	3	AgCuSi	none	2,570	2,430	22	none		1,040	3
AgCuTi	none	2,740	1,910	41	none		1,150	3	AgCuV	none	5,000	2,610	41	none		1,110	3
AgCuZr	none	1,130	1,660	48	none		1,040	3	AgFeNi	none	6,920	2,830	25	none		1,230	3
AgFePd	none	4,320	1,990	43	none		1,320	3	AgHfZr	fcc	1,210	1,150	44	bcc	1,360	1,710	2
AgIrNi	none	6,630	2,850	30	none		1,230	3	AgIrPd	none	6,110	2,560	35	none		1,530	3
AgIrPt	none	4,960	2,270	29	none		1,390	3	AgIrRh	none	6,770	2,640	25	none		1,230	3
AgNiPd	none	3,730	1,430	14	none		1,430	3	AgNiPt	none	3,270	1,530	26	none		1,310	2

	S.S.	T_c	$\tilde{T}_c$	CV	S.S.$^{(\star)}$	$T_c^{(\star)}$	$T_m^{(\star)}$	$n^{(\star)}$		S.S.	T_c	$\tilde{T}_c$	CV	S.S.$^{(\star)}$	$T_c^{(\star)}$	$T_m^{(\star)}$	$n^{(\star)}$
AgNiRh	none	4,900	2,110	20	none		1,230	2	AgPdPt	fcc	480	440	8	fcc	1,170	1,610	2
AgPdRh	none	3,850	1,580	12	none		1,530	3	AgPdV	none	4,530	2,260	41	none		1,490	2
AgPtRh	none	3,090	1,340	14	none		1,300	3	AgPtRu	fcc	790	2,510	35	none		1,260	3
AgPtTi	none	5,440	3,410	44	none		1,230	3	AgPtV	none	6,980	3,770	48	none		1,360	2
AgTiV	none	4,010	2,530	46	none		1,230	3	AgTiZr	none	3,840	1,710	45	bcc	1,120	1,540	3
AlAuCu	none	1,400	1,730	41	fcc	750	960	3	AlAuNi	none	3,810	2,230	47	none		1,050	3
AlAuSi	none	3,340	3,540	46	none		780	3	AlCoCr	none	6,620	3,660	47	none		1,520	3
AlCoCu	none	2,400	2,000	42	none		1,320	3	AlCoNi	none	2,400	3,290	48	none		1,440	3
AlCrCu	none	3,670	2,310	50	none		1,200	3	AlCrMn	none	1,610	1,480	46	bcc	273	1,590	3
AlCrV	none	2,160	1,130	48	bcc	273	1,970	3	AlCrW	none	2,380	1,580	43	none		1,600	3
AlCuFe	none	3,140	1,960	47	none		1,310	3	AlCuMn	none	2,690	1,630	50	bcc	880	1,310	3
AlCuNi	none	3,360	2,180	34	none		1,340	3	AlCuSi	none	2,330	2,380	18	none		840	3
AlFeMn	none	3,000	1,420	49	none		1,570	3	AlHfSi	none	2,390	3,740	49	none		930	2
AlHfTa	none	2,530	1,750	39	none		1,570	2	AlHfTi	fcc	1,000	1,600	34	bcc	1,600	1,730	2
AlMnNi	none	2,760	2,230	48	none		1,350	2	AlMnSi	none	2,720	3,300	47	none		1,110	3
AlTaZr	none	3,190	2,150	45	none		1,580	3	AlTiV	none	2,820	1,820	39	bcc	1,010	2,000	3
AlTiZr	fcc	1,630	1,830	49	bcc	1,420	1,650	3	AlVW	none	2,490	1,180	49	bcc	2,060	2,080	3
AsAuCu	none	1,750	1,710	34	none		920	2	AsAuPd	none	2,620	2,080	45	none		1,010	2
AsCuPd	none	1,660	1,560	43	none		1,020	1	AuCoCu	none	3,970	1,800	36	none	720	1,640	3
AuCoIr	none	6,600	2,520	29	fcc	1,500	1,880	1	AuCoMo	none	5,050	2,930	39	none		1,500	2
AuCoNi	none	3,060	1,740	43	none		1,300	3	AuCoPd	none	3,710	1,600	15	fcc	1,350	1,450	3
AuCoPt	none	3,610	1,680	16	none		1,520	2	AuCoRh	none	4,040	1,760	17	none		1,590	2
AuCoV	none	3,630	1,940	38	none	1,290	1,480	2	AuCuFe	none	3,850	1,620	38	none		1,220	2
AuCuIr	none	5,170	2,290	29	none		1,270	2	AuCuNi	none	1,980	900	16	fcc	1,120	1,250	3
AuCuPd	bcc	970	700	22	fcc	273	1,440	3	AuCuPt	fcc	1,330	880	12	fcc	273	1,440	1
AuCuRh	none	2,620	1,190	16	none		1,190	3	AuCuSi	none	2,910	1,660	39	none		750	3
AuCuTi	none	1,330	1,570	41	none		1,210	3	AuCuV	fcc	1,240	1,340	34	none		1,570	2
AuCuW	none	3,280	3,690	48	none		1,230	1	AuFeNi	none	3,050	1,560	43	fcc	880	1,420	2
AuFePd	fcc	1,060	960	46	fcc	710	1,600	2	AuHfTi	fcc	270	1,420	48	none		1,270	3
AuIrNi	none	5,090	2,360	30	fcc	800	1,690	2	AuIrPd	none	5,930	2,620	25	fcc	1,290	1,960	2
AuIrPt	none	4,850	2,040	23	fcc	1,050	1,850	1	AuIrRh	none	5,960	2,280	23	none		1,830	2
AuMoNi	none	4,100	2,490	43	none		1,290	2	AuMoPd	none	1,750	1,910	38	none		1,680	2
AuMoRh	none	5,400	2,630	35	none		1,670	1	AuNiPd	none	2,610	1,100	15	fcc	810	1,440	3
AuNiPt	none	2,350	1,210	27	fcc	800	1,530	1	AuNiRh	none	2,880	1,380	17	none		1,250	2
AuNiV	none	2,730	1,690	37	fcc	1,110	1,250	2	AuPdPt	fcc	1,200	650	6	fcc	273	1,790	1
AuPdRh	none	3,340	1,450	11	none		1,700	3	AuPdTi	none	1,740	1,910	43	fcc	1,580	1,630	2
AuPdV	fcc	750	1,000	31	none		1,540	1	AuPdW	none	2,230	2,510	50	none		1,770	1
AuPtRh	none	2,590	1,110	10	none		1,550	2	AuPtRu	none	4,320	2,090	32	none		1,510	2
AuPtTi	none	1,970	2,820	46	none		1,670	2	AuRhV	none	3,650	2,240	42	none		1,400	1
AuRhW	none	6,630	3,170	46	none		1,790	1	AuTaTi	fcc	1,180	1,430	48	none		1,710	2
AuTiV	fcc	1,540	1,870	44	none		1,670	2	AuTiZr	fcc	410	1,540	47	fcc	1,210	1,390	3
CoCrCu	none	3,920	2,090	35	none		1,590	3	CoCrIr	fcc	1,660	1,780	26	fcc	970	1,970	1
CoCrMn	none	3,080	1,550	41	bcc	1,320	1,510	3	CoCrNb	none	3,370	2,170	46	none		1,430	3
CoCrNi	fcc	1,350	890	28	fcc	970	1,670	3	CoCrPd	none	3,210	2,040	39	fcc	990	1,540	3
CoCrPt	none	2,030	1,390	38	fcc	890	1,820	3	CoCrRh	fcc	1,610	1,330	29	fcc	1,110	1,820	1
CoCrW	none	3,330	1,930	49	none		1,680	3	CoCuIr	none	2,640	1,260	28	none		1,750	2
CoCuMn	none	2,410	1,520	40	none		1,180	3	CoCuNi	bcc	1,400	1,120	35	none		1,600	3
CoCuPd	none	3,020	1,610	21	fcc	1,420	1,460	3	CoCuPt	none	2,050	1,310	22	none		1,460	2
CoCuRh	none	1,720	1,020	14	none		1,670	2	CoCuV	none	3,430	1,970	41	none		2,090	3
CoFeMn	none	2,770	1,300	49	fcc	790	1,550	3	CoIrMn	none	2,110	1,540	19	fcc	273	1,820	1
CoIrMo	none	2,860	2,160	29	fcc	1,180	2,110	1	CoIrNi	fcc	1,040	730	22	fcc	740	2,030	2
CoIrPd	none	1,850	1,080	20	fcc	1,550	1,650	2	CoIrPt	fcc	1,670	950	19	fcc	1,280	1,910	2
CoIrRh	fcc	1,250	520	13	fcc	690	2,150	1	CoIrV	none	3,520	2,090	47	fcc	1,290	1,650	1

	S.S.	T_c	$\tilde{T}_c$	CV	S.S.$^{(\star)}$	$T_c^{(\star)}$	$T_m^{(\star)}$	$n^{(\star)}$		S.S.	T_c	$\tilde{T}_c$	CV	S.S.$^{(\star)}$	$T_c^{(\star)}$	$T_m^{(\star)}$	$n^{(\star)}$
CoIrW	none	3,110	2,350	35	none		2,070	1	CoMnNi	none	2,100	1,070	30	fcc	600	1,440	2
CoMnRh	none	2,020	1,920	29	fcc	273	1,710	1	CoMoNi	fcc	1,130	1,560	41	none		1,600	3
CoMoPt	fcc	1,250	1,780	45	none		1,740	2	CoMoRh	none	2,140	1,980	38	fcc	1,370	1,920	1
CoNiPd	fcc	1,430	710	28	fcc	273	1,520	3	CoNiPt	fcc	800	590	22	fcc	620	1,780	2
CoNiRh	fcc	1,340	630	19	fcc	740	1,900	1	CoNiV	none	2,750	1,450	38	fcc	750	1,490	3
CoPdPt	fcc	1,030	670	14	fcc	670	1,650	2	CoPdRh	fcc	1,520	940	23	fcc	1,080	1,670	2
CoPdV	none	2,430	1,780	41	none		1,400	2	CoPdW	none	2,780	1,800	48	none		1,550	2
CoPtRh	fcc	1,060	650	15	fcc	610	1,960	2	CoPtV	none	2,200	1,920	50	fcc	1,310	1,500	2
CoRhV	none	3,120	1,910	42	fcc	1,290	1,570	1	CoRhW	none	3,310	2,220	35	none		1,920	1
CrCuFe	none	4,540	2,320	40	none		1,350	3	CrCuMo	none	5,520	2,630	50	none		1,340	3
CrCuNi	none	2,770	1,750	26	none		1,390	3	CrCuPd	none	3,050	2,210	41	none		1,440	3
CrCuPt	none	2,220	1,890	41	none		1,360	2	CrCuRh	none	3,260	1,700	46	none		1,390	2
CrCuV	none	4,980	2,220	38	none		1,570	3	CrCuW	none	6,620	3,060	45	none		1,770	2
CrFeIr	fcc	1,860	1,550	33	fcc	1,050	1,970	1	CrFeMn	bcc	1,040	800	25	bcc	1,380	1,690	3
CrFeMo	none	2,300	1,350	26	none	1,400	2,030	3	CrFeNb	none	2,460	1,900	29	none		1,450	3
CrFeNi	none	2,860	1,530	48	fcc	1,230	1,660	3	CrFeRh	none	2,170	1,500	42	fcc	1,220	1,780	1
CrFeTa	none	3,740	2,610	32	none		1,660	3	CrFeTi	none	4,920	2,940	41	none		1,470	3
CrFeV	bcc	1,830	1,070	23	bcc	1,160	1,900	3	CrFeW	none	2,300	1,440	37	none		1,930	3
CrHfNb	none	3,130	2,300	30	bcc	1,410	2,040	2	CrHfTa	bcc	2,060	2,530	31	bcc	1,660	2,220	2
CrHfTi	none	2,010	2,290	40	bcc	1,000	1,900	2	CrHfW	none	2,950	3,270	32	none		2,190	2
CrIrMn	none	3,320	1,930	43	fcc	1,720	1,770	1	CrIrNi	fcc	1,620	1,200	29	fcc	930	1,930	2
CrIrPd	none	3,490	2,340	45	fcc	1,470	1,780	2	CrIrPt	none	2,270	1,820	32	none		2,010	2
CrIrRh	fcc	1,100	1,180	24	fcc	690	1,960	1	CrMnMo	none	2,150	1,530	16	bcc	1,690	1,830	3
CrMnNb	none	3,690	2,100	25	bcc	1,500	1,780	2	CrMnNi	none	3,170	1,410	45	none		1,400	2
CrMnRh	none	3,100	2,030	47	none		1,700	1	CrMnTa	none	4,900	2,590	23	bcc	1,790	1,880	2
CrMnTi	none	2,970	2,150	44	none	273	1,740	3	CrMnV	none	2,630	1,380	15	bcc	640	1,860	3
CrMnW	none	2,230	1,660	18	none		2,170	3	CrMoNb	none	3,150	1,380	6	bcc	1,680	2,090	3
CrMoRe	bcc	1,170	1,040	22	bcc	2,030	2,410	1	CrMoTa	none	2,780	1,800	9	bcc	2,010	2,030	3
CrMoTc	bcc	1,230	1,050	12	bcc	1,930	2,150	1	CrMoTi	bcc	1,930	1,580	27	bcc	1,390	1,940	3
CrMoV	bcc	1,260	790	4	bcc	1,280	2,310	3	CrMoW	bcc	2,260	820	5	bcc	1,410	2,510	3
CrMoZr	none	3,850	2,610	30	none		1,980	3	CrNbTa	none	2,250	1,370	9	none		2,000	3
CrNbTi	none	1,980	1,460	19	none		1,690	3	CrNbV	none	2,520	1,210	7	bcc	1,290	1,950	3
CrNbW	none	2,930	1,260	8	bcc	1,910	1,990	3	CrNbZr	none	3,540	2,200	27	none		1,640	3
CrNiPd	none	2,220	1,650	36	fcc	960	1,540	3	CrNiPt	fcc	1,560	1,320	33	fcc	1,700	1,790	2
CrNiRh	fcc	1,430	1,130	30	fcc	970	1,810	1	CrPdPt	none	2,390	1,620	40	none		1,790	2
CrPdRh	none	2,550	1,750	40	fcc	1,190	1,740	2	CrPtRh	none	2,120	1,360	33	fcc	1,960	2,040	2
CrReTa	none	4,530	2,710	24	bcc	2,110	2,310	1	CrReW	bcc	1,010	1,000	24	bcc	1,850	2,600	1
CrTaTi	bcc	1,420	1,640	26	none		1,760	3	CrTaV	bcc	1,700	1,790	8	bcc	1,800	2,120	3
CrTaW	bcc	2,320	1,690	10	bcc	2,050	2,390	3	CrTaZr	none	2,980	2,670	28	none		1,630	3
CrTcW	bcc	1,030	990	17	bcc	1,780	2,250	1	CrTiV	bcc	1,150	1,040	15	bcc	1,060	1,640	3
CrTiW	bcc	1,470	1,540	18	none		1,930	3	CrTiZr	none	3,970	2,280	49	none		1,570	3
CrVW	bcc	1,220	760	7	bcc	1,670	2,330	3	CrWZr	none	3,580	3,080	29	none		1,750	3
CuFeMn	none	2,830	1,700	47	none		1,180	3	CuFeNi	none	1,670	960	19	fcc	1,340	1,510	3
CuFePd	fcc	1,360	930	30	none		1,430	3	CuFeRh	none	2,340	1,070	44	none		1,420	2
CuFeV	none	3,750	1,850	37	none		1,470	3	CuHfTi	fcc	730	1,170	42	none		1,050	3
CuHfZr	fcc	560	1,210	48	none		990	3	CuIrMn	none	2,610	2,020	41	none		1,210	2
CuIrNi	fcc	1,150	970	21	none		1,530	3	CuIrPd	none	3,260	1,650	25	none		1,530	3
CuIrPt	none	2,800	1,530	23	none		1,610	2	CuIrRh	none	1,760	860	22	none		1,520	3
CuMnNi	none	2,290	1,400	38	fcc	1,080	1,270	2	CuNiPd	none	1,680	920	12	fcc	510	1,500	3
CuNiPt	fcc	940	750	13	fcc	273	1,690	1	CuNiRh	fcc	1,100	610	13	fcc	1,180	1,650	2
CuNiSi	none	3,310	2,430	41	none		1,100	3	CuNiV	none	2,400	1,440	38	none		1,490	3
CuPdPt	fcc	650	460	9	fcc	540	1,670	1	CuPdRh	none	2,230	1,140	13	fcc	1,510	1,610	3
CuPdTi	none	1,400	1,750	45	fcc	920	1,350	2	CuPdV	fcc	1,310	1,150	38	none		1,470	2

	S.S.	T_c	$\tilde{T}_c$	CV	S.S.$^{(\star)}$	$T_c^{(\star)}$	$T_m^{(\star)}$	$n^{(\star)}$		S.S.	T_c	$\tilde{T}_c$	CV	S.S.$^{(\star)}$	$T_c^{(\star)}$	$T_m^{(\star)}$	$n^{(\star)}$
CuPtRh	fcc	1,450	930	14	fcc	1,120	1,800	2	CuPtRu	none	2,790	1,520	31	fcc	1,680	1,870	1
CuPtTi	none	2,050	2,530	46	none		1,310	2	CuPtV	none	3,060	2,220	45	none		1,600	1
CuRhV	none	3,410	1,920	44	none		1,570	2	CuTaTi	fcc	1,510	1,710	46	bcc	1,140	1,530	2
CuTaV	none	2,740	2,140	49	none		1,820	2	CuTiV	none	1,560	1,750	42	none		1,190	3
CuTiZr	none	2,230	1,440	39	none		980	3	CuVW	none	5,530	2,350	49	bcc	1,870	1,970	2
FeIrMn	none	2,340	1,520	34	fcc	273	1,920	1	FeIrMo	none	3,140	1,820	44	none		2,020	1
FeIrNi	fcc	1,100	880	34	fcc	570	2,040	2	FeIrRh	fcc	1,420	740	43	fcc	690	2,180	1
FeIrRu	none	2,850	1,240	33	fcc	1,800	2,380	2	FeMnMo	none	2,050	1,620	32	none		1,510	3
FeMnNb	none	3,330	2,330	35	none		1,530	2	FeMnNi	none	1,830	1,120	37	fcc	550	1,500	2
FeMnRh	none	2,360	1,800	41	fcc	273	1,790	1	FeMnTa	none	4,650	2,740	37	none		1,650	2
FeMnTi	none	5,170	2,490	48	none	273	1,590	3	FeMnV	none	2,820	1,400	25	bcc	1,440	1,670	3
FeMoNb	none	2,880	1,550	38	none		1,650	3	FeMoNi	fcc	1,080	1,480	47	none		1,630	3
FeMoPd	none	2,130	1,520	49	none		1,530	3	FeMoRh	none	2,500	1,630	46	none		1,890	1
FeMoTa	none	3,200	1,810	41	none		1,730	3	FeMoTi	none	4,780	2,540	47	none		1,530	3
FeMoV	none	2,260	1,180	31	bcc	1,590	1,940	3	FeMoW	none	2,930	1,540	50	none		1,930	3
FeNbTa	none	2,200	1,210	32	none		1,610	3	FeNbTi	none	4,840	2,620	40	none		1,320	3
FeNbV	none	2,000	1,210	27	none		1,540	3	FeNiRh	none	2,000	1,250	38	fcc	550	1,900	1
FeTaTi	none	4,700	2,640	43	none		1,350	3	FeTaV	none	2,170	1,730	31	none		1,670	3
FeTaW	none	3,200	1,730	47	none		1,960	3	FeTiV	none	4,650	2,180	33	bcc	1,310	1,480	3
FeVW	none	2,590	1,260	39	none		1,880	3	HfMoNb	bcc	1,760	980	20	bcc	1,370	2,280	3
HfMoRe	none	4,440	2,600	48	bcc	2,310	2,350	1	HfMoTa	bcc	1,720	1,510	25	bcc	1,640	2,280	3
HfMoTi	bcc	1,890	1,120	31	bcc	1,030	2,100	3	HfMoV	bcc	2,100	1,440	37	bcc	1,470	2,290	2
HfMoW	none	3,340	2,190	36	none		2,540	3	HfMoZr	none	5,670	3,400	42	bcc	1,860	1,990	3
HfNbTa	bcc	640	860	9	bcc	1,370	2,490	3	HfNbTi	bcc	1,320	880	23	bcc	1,110	2,130	3
HfNbV	bcc	1,670	1,700	23	bcc	1,090	2,240	2	HfNbW	bcc	940	1,100	18	bcc	2,040	2,250	3
HfNbZr	bcc	1,730	1,180	29	bcc	1,250	2,190	3	HfReTa	none	4,520	2,350	38	bcc	2,180	2,610	1
HfTaTc	bcc	1,560	2,640	44	bcc	2,100	2,300	1	HfTaTi	bcc	1,840	1,230	19	bcc	1,150	2,200	3
HfTaV	bcc	1,790	2,080	18	bcc	1,170	2,380	2	HfTaW	bcc	1,280	1,410	17	bcc	1,960	2,320	3
HfTaZr	bcc	2,200	1,480	22	bcc	1,630	2,250	3	HfTiV	bcc	1,690	1,490	31	bcc	870	2,050	2
HfTiW	bcc	1,580	1,730	29	none		2,110	3	HfTiZr	bcc	1,630	1,270	36	bcc	1,240	2,000	3
HfVW	bcc	2,110	1,620	44	bcc	2,190	2,270	2	HfVZr	none	2,570	1,930	33	bcc	1,400	1,920	2
HfWZr	none	4,900	2,870	43	none		2,050	3	IrMnNi	none	2,410	1,720	29	fcc	740	1,690	1
IrMnRh	none	1,990	1,500	34	fcc	690	1,990	1	IrMoNi	none	2,680	1,660	37	none		1,950	2
IrMoPd	none	3,070	2,020	33	fcc	1,670	2,230	2	IrMoPt	fcc	1,660	2,410	50	none		2,030	1
IrNbPd	none	2,410	3,130	49	none		1,860	1	IrNiPd	none	1,830	1,140	21	fcc	1,330	1,670	3
IrNiPt	fcc	1,470	830	23	fcc	1,050	2,010	2	IrNiRh	fcc	730	490	17	fcc	700	2,090	2
IrNiRu	fcc	1,470	970	17	fcc	1,520	2,430	3	IrNiW	none	2,440	1,820	44	none		1,980	2
IrOsPt	fcc	1,480	1,010	14	fcc	1,830	2,620	1	IrPdPt	fcc	1,990	940	12	fcc	1,450	2,020	2
IrPdRh	fcc	1,980	880	12	fcc	1,280	2,090	3	IrPdRu	none	2,840	1,440	17	fcc	1,820	2,150	3
IrPdV	none	2,950	2,210	46	fcc	1,220	1,730	1	IrPdW	none	3,280	2,470	41	none		2,210	1
IrPtRe	fcc	1,610	1,510	26	fcc	1,790	2,410	1	IrPtRh	fcc	500	470	6	fcc	1,310	2,190	3
IrPtRu	fcc	1,120	690	12	fcc	990	2,630	3	IrPtTc	fcc	1,520	1,340	20	fcc	1,540	2,110	1
IrRhV	none	3,770	1,920	45	fcc	790	1,780	1	MnMoNb	none	3,210	1,630	25	bcc	1,430	2,220	2
MnMoTa	none	4,340	1,940	24	bcc	1,770	2,070	2	MnMoTi	none	2,970	1,860	30	none		1,550	3
MnMoV	none	3,020	1,610	21	bcc	1,550	2,010	3	MnMoW	bcc	2,000	1,660	20	none	1,970	2,010	3
MnNbTa	none	5,070	2,040	25	bcc	273	2,460	1	MnNbTi	none	3,580	2,320	41	bcc	980	1,830	2
MnNbV	none	3,330	1,950	21	bcc	273	2,010	2	MnNbW	none	3,410	1,590	25	none		1,780	2
MnTaTi	none	4,810	1,940	35	bcc	990	1,910	2	MnTaV	none	4,400	2,070	18	bcc	670	2,110	2
MnTaW	none	4,510	2,110	31	none		1,880	2	MnTiV	none	2,930	2,440	42	bcc	850	1,640	3
MnTiW	none	3,900	2,530	40	none	1,850	2,330	3	MnVW	none	3,030	1,680	22	none		1,820	3
MoNbRe	bcc	2,540	1,410	14	bcc	1,840	2,790	1	MoNbTa	bcc	1,080	660	4	bcc	273	2,910	3
MoNbTc	none	3,590	1,820	16	bcc	1,790	2,410	1	MoNbTi	bcc	790	560	14	bcc	990	2,430	3
MoNbV	bcc	940	680	5	bcc	1,310	2,430	3	MoNbW	bcc	690	540	3	bcc	273	3,030	3

	S.S.	T_c	$\tilde{T}_c$	CV	S.S.$^{(\star)}$	$T_c^{(\star)}$	$T_m^{(\star)}$	$n^{(\star)}$		S.S.	T_c	$\tilde{T}_c$	CV	S.S.$^{(\star)}$	$T_c^{(\star)}$	$T_m^{(\star)}$	$n^{(\star)}$
MoNbZr	none	2,570	1,810	20	bcc	1,810	1,930	3	MoNiPd	none	1,640	1,450	42	none		1,400	3
MoNiPt	fcc	1,060	1,280	47	none		1,760	1	MoNiRh	fcc	1,650	1,650	37	none		1,830	1
MoPdPt	fcc	1,660	1,420	43	fcc	1,700	1,920	1	MoPdRh	fcc	1,780	1,600	32	fcc	1,590	2,000	2
MoReTa	none	3,950	1,950	23	bcc	2,100	2,950	1	MoReTi	bcc	1,310	1,740	28	bcc	2,030	2,430	1
MoReV	bcc	1,740	1,310	18	bcc	1,950	2,520	1	MoReW	bcc	820	880	7	bcc	1,620	3,150	1
MoTaTc	none	4,830	2,400	23	bcc	2,040	2,480	1	MoTaTi	bcc	810	810	14	bcc	1,310	2,480	3
MoTaV	bcc	1,200	1,070	4	bcc	1,790	2,440	3	MoTaW	bcc	730	840	5	bcc	273	3,200	3
MoTaZr	none	2,560	1,760	24	none		1,970	3	MoTcTi	none	2,750	1,980	29	bcc	1,950	2,130	1
MoTcV	none	2,500	1,540	14	bcc	1,870	2,230	1	MoTcW	bcc	1,000	710	12	bcc	1,580	2,710	1
MoTiV	bcc	950	650	16	bcc	1,110	2,220	3	MoTiW	bcc	800	750	18	bcc	820	2,580	3
MoTiZr	bcc	1,160	1,200	25	bcc	1,210	1,840	3	MoVW	bcc	410	480	7	bcc	1,040	2,720	3
MoVZr	none	3,650	2,000	40	bcc	1,530	1,670	3	MoWZr	none	2,470	2,170	40	none		1,830	3
NbPdRh	fcc	1,470	2,540	49	none		1,790	1	NbReTa	none	4,180	1,710	33	bcc	1,560	2,920	1
NbReTi	bcc	2,030	1,420	27	bcc	2,130	2,290	1	NbReV	bcc	1,890	1,560	24	bcc	1,700	2,300	1
NbReW	bcc	2,620	1,530	16	bcc	1,740	3,050	1	NbReZr	none	2,940	1,920	32	bcc	2,180	2,220	1
NbTaTc	none	5,400	1,990	31	bcc	1,530	2,500	1	NbTaTi	bcc	640	460	4	bcc	820	2,430	3
NbTaV	bcc	1,410	990	3	bcc	900	2,400	3	NbTaW	bcc	300	320	5	bcc	273	3,160	3
NbTaZr	bcc	1,470	940	8	bcc	1,590	2,170	3	NbTcV	none	3,400	1,770	22	bcc	1,660	2,060	1
NbTcW	none	3,600	1,940	22	bcc	1,700	2,620	1	NbTiV	bcc	1,110	990	9	bcc	650	2,030	3
NbTiW	bcc	360	450	13	bcc	1,420	2,400	3	NbTiZr	bcc	1,330	850	19	bcc	930	1,960	3
NbVW	bcc	880	620	6	bcc	1,180	2,500	3	NbVZr	none	2,140	1,710	16	bcc	1,510	1,700	3
NbWZr	none	2,390	1,380	17	none		1,980	3	NiPdPt	fcc	1,110	640	12	fcc	273	1,670	1
NiPdRh	fcc	1,190	720	12	fcc	900	1,670	2	NiPdV	none	1,690	1,600	36	fcc	1,130	1,450	2
NiPtRh	fcc	1,050	630	11	fcc	273	2,020	1	NiPtRu	fcc	1,250	890	16	fcc	1,030	2,060	2
NiPtV	fcc	1,480	1,900	42	fcc	1,090	1,630	1	NiRhV	none	3,260	1,840	42	fcc	1,090	1,680	1
NiRhW	fcc	1,750	1,910	42	none		1,880	1	PdPtRh	fcc	830	470	4	fcc	810	2,040	2
PdPtRu	fcc	1,170	970	20	fcc	1,250	2,060	2	PdPtTi	fcc	1,030	2,900	39	none		1,780	1
PdRhV	fcc	1,520	1,740	40	fcc	1,130	1,650	1	PdRhW	fcc	1,740	1,800	40	none		2,050	1
PdRuW	fcc	2,220	1,760	39	bcc	1,740	2,480	1	PdTiV	none	2,340	1,620	48	bcc	1,430	1,520	1
PtRhRu	fcc	770	530	9	fcc	940	2,290	2	PtRhV	none	2,080	1,860	45	none		1,760	1
PtRhW	fcc	1,410	2,000	45	none		2,190	1	ReTaTi	none	2,980	1,680	30	bcc	2,120	2,430	1
ReTaV	none	3,520	1,990	24	bcc	1,740	2,500	1	ReTaW	none	3,920	2,110	21	bcc	1,670	3,340	1
ReTaZr	none	4,120	2,440	35	bcc	2,220	2,320	1	ReTiW	bcc	2,320	1,870	31	bcc	2,140	2,540	1
ReVW	bcc	1,760	1,400	16	bcc	1,770	2,670	1	TaTcTi	none	4,680	2,080	31	bcc	2,020	2,120	1
TaTcV	none	4,420	2,130	26	bcc	1,700	2,190	1	TaTcW	none	5,010	2,580	22	bcc	1,640	2,820	1
TaTiV	bcc	1,380	1,450	7	bcc	870	2,110	3	TaTiW	bcc	710	670	16	bcc	1,250	2,540	3
TaTiZr	bcc	1,330	1,110	17	bcc	1,410	1,980	3	TaVW	bcc	750	880	7	bcc	1,090	2,680	3
TaVZr	none	1,940	2,210	16	none		1,670	3	TaWZr	none	2,880	1,690	17	none		2,050	3
TcTiW	none	3,140	2,250	37	bcc	2,030	2,230	1	TcVW	none	2,440	1,590	17	bcc	1,720	2,340	1
TiVZr	none	2,200	1,580	40	bcc	1,330	1,550	3	TiWZr	none	1,960	1,730	24	none		1,880	3
VWZr	none	3,710	2,040	28	none		1,640	3									

C. Quaternary alloys at equi-composition

TABLE V: LTVC results for quaternary alloys. S.S. type of single solid solution phase ("none" = not found); T_c (K) transition temperature, as estimated by the method; $\tilde{T}_c$ (K) approximated transition temperature, estimated according to Eq. (8); CV (meV) cluster expansion cross validation score; $\bar{T}_m$ (K) melting temperature (solidus), calculated as the average of the melting temperatures at equi-composition of the 6 binary alloys associated with the quaternary alloy; A solid solution is predicted if $T_c < \bar{T}_m$.

	S.S.	T_c	$\tilde{T}_c$	$\bar{T}_m$	CV		S.S.	T_c	$\tilde{T}_c$	$\bar{T}_m$	CV		S.S.	T_c	$\tilde{T}_c$	$\bar{T}_m$	CV
AgAlAuCo	none	5,000	5,000	1,320	36	AgAlAuCu	fcc	980	1,120	1,220	24	AgAlAuFe	none	3,620	4,360	1,330	41
AgAlAuNi	none	5,000	5,000	1,310	32	AgAlAuSi	none	2,640	3,040	1,300	29	AgAlAuZr	none	2,700	1,840	1,410	50
AgAlCoCu	none	5,000	5,000	1,320	34	AgAlCoNi	none	5,000	5,000	1,420	42	AgAlCuFe	none	3,160	1,980	1,330	32
AgAlCuMn	none	3,400	1,760	1,260	50	AgAlCuNi	none	5,000	5,000	1,310	28	AgAlCuSi	none	3,340	3,540	1,300	19
AgAlCuZr	none	2,260	2,440	1,410	48	AgAlFeNi	none	5,000	5,000	1,430	46	AgAlNiSi	none	1,780	3,220	1,390	46
AgAuCoCr	none	5,000	5,000	1,620	50	AgAuCoCu	none	5,000	5,000	1,320	19	AgAuCoIr	fcc	340	2,640	1,760	35
AgAuCoMo	none	5,000	5,000	1,810	43	AgAuCoNi	fcc	420	2,140	1,470	27	AgAuCoPd	none	5,000	5,000	1,460	16
AgAuCoPt	none	1,640	1,800	1,520	22	AgAuCoRe	none	5,000	5,000	1,950	50	AgAuCoRh	fcc	1,080	2,040	1,640	20
AgAuCoRu	none	5,000	5,000	1,730	37	AgAuCrCu	none	5,000	5,000	1,510	50	AgAuCrNi	fcc	660	2,420	1,610	50
AgAuCuFe	fcc	1,040	1,580	1,430	35	AgAuCuIr	none	5,000	5,000	1,650	33	AgAuCuNi	fcc	600	1,100	1,350	14
AgAuCuPd	fcc	980	720	1,380	8	AgAuCuPt	none	2,320	1,040	1,450	13	AgAuCuRh	none	4,220	1,240	1,540	15
AgAuCuRu	none	5,000	5,000	1,630	39	AgAuCuSi	none	3,260	1,660	1,400	22	AgAuCuZr	none	2,100	1,520	1,510	47
AgAuFeMo	none	5,000	5,000	1,820	46	AgAuFeNi	none	5,000	5,000	1,530	39	AgAuFePd	fcc	1,480	1,200	1,550	35
AgAuFeRh	fcc	740	2,160	1,650	48	AgAuIrMo	none	5,000	5,000	2,040	49	AgAuIrNi	none	5,000	5,000	1,750	31
AgAuIrPd	fcc	260	2,040	1,770	28	AgAuIrPt	fcc	960	1,920	1,830	26	AgAuIrRh	none	5,000	5,000	1,870	36
AgAuIrRu	none	5,000	5,000	1,960	47	AgAuMoNi	none	5,000	5,000	1,800	39	AgAuMoPd	fcc	1,180	1,920	1,820	36
AgAuMoRh	none	5,000	5,000	1,930	40	AgAuNbRh	none	5,000	5,000	1,890	50	AgAuNiPd	none	3,640	1,040	1,520	13
AgAuNiPt	none	2,080	1,340	1,570	13	AgAuNiRe	fcc	780	3,360	1,940	50	AgAuNiRh	fcc	1,040	1,660	1,630	23
AgAuNiRu	none	5,000	5,000	1,720	40	AgAuNiSi	none	5,000	5,000	1,500	42	AgAuPdPt	fcc	1,020	540	1,630	7
AgAuPdRe	fcc	420	2,740	1,960	46	AgAuPdRh	none	5,000	5,000	1,660	14	AgAuPdRu	fcc	280	2,200	1,750	34
AgAuPtRh	fcc	740	1,180	1,710	13	AgAuPtRu	fcc	1,620	2,080	1,800	46	AgAuRhRu	fcc	540	2,520	1,850	34
AgCoCrCu	none	5,000	5,000	1,620	48	AgCoCrNi	none	5,000	5,000	1,710	39	AgCoCrOs	none	5,000	5,000	2,110	50
AgCoCrPd	none	5,000	5,000	1,740	42	AgCoCrPt	none	5,000	5,000	1,790	42	AgCoCrRh	none	5,000	5,000	1,840	44
AgCoCrRu	none	5,000	5,000	1,930	45	AgCoCuFe	none	5,000	5,000	1,540	47	AgCoCuPd	none	5,000	5,000	1,410	23
AgCoCuPt	none	2,920	1,660	1,560	23	AgCoIrMo	none	5,000	5,000	2,140	48	AgCoIrPd	fcc	280	2,080	1,880	28
AgCoIrPt	fcc	1,660	1,920	1,930	27	AgCoMoNi	none	5,000	5,000	1,900	43	AgCoMoOs	none	5,000	5,000	2,300	50
AgCoMoPd	fcc	1,140	2,380	1,930	38	AgCoMoPt	none	5,000	5,000	1,980	42	AgCoMoRe	none	5,000	5,000	2,340	50
AgCoMoRh	none	5,000	5,000	2,030	45	AgCoMoRu	none	5,000	5,000	2,120	39	AgCoNiPd	fcc	680	1,740	1,550	26
AgCoNiPt	none	5,000	5,000	1,680	30	AgCoOsPd	none	5,000	5,000	2,040	44	AgCoOsPt	none	5,000	5,000	2,090	43
AgCoPdPt	fcc	1,420	1,300	1,620	17	AgCoPdRe	fcc	960	2,840	2,070	37	AgCoPdRh	fcc	1,400	1,640	1,770	24
AgCoPdRu	none	5,000	5,000	1,850	30	AgCoPtRe	fcc	1,020	2,340	2,130	41	AgCoPtRh	fcc	1,260	1,560	1,820	26
AgCoPtRu	none	5,000	5,000	1,910	35	AgCrCuFe	none	5,000	5,000	1,630	47	AgCrCuNi	none	5,000	5,000	1,610	36
AgCrCuPd	none	4,020	2,080	1,640	42	AgCrCuPt	none	5,000	5,000	1,690	43	AgCrCuRh	none	5,000	5,000	1,740	46
AgCrCuRu	none	5,000	5,000	1,830	50	AgCrFeNi	none	5,000	5,000	1,720	47	AgCrIrNi	none	5,000	5,000	1,940	45
AgCrIrPd	none	5,000	5,000	1,970	49	AgCrIrRh	none	5,000	5,000	2,070	47	AgCrIrRu	fcc	460	3,040	2,160	50
AgCrNiOs	none	5,000	5,000	2,100	50	AgCrNiPd	none	1,760	2,000	1,730	39	AgCrNiPt	none	5,000	5,000	1,780	39
AgCrNiRh	none	5,000	5,000	1,830	43	AgCrNiRu	none	5,000	5,000	1,920	45	AgCrOsPt	none	5,000	5,000	2,180	50
AgCrPdPt	none	5,000	5,000	1,810	43	AgCrPdRh	none	5,000	5,000	1,860	47	AgCrPdRu	none	5,000	5,000	1,940	49
AgCrPtRh	none	5,000	5,000	1,910	45	AgCrPtRu	fcc	460	2,460	2,000	47	AgCrRhRu	fcc	240	2,380	2,050	49
AgCuFeIr	none	2,180	2,060	1,770	49	AgCuFeNi	none	5,000	5,000	1,600	20	AgCuFeOs	fcc	1,120	2,860	1,930	50
AgCuFePd	fcc	1,420	1,280	1,530	27	AgCuFeRe	none	5,000	5,000	1,960	42	AgCuFeRh	none	5,000	5,000	1,660	45
AgCuFeRu	none	5,000	5,000	1,750	43	AgCuIrPd	none	5,000	5,000	1,780	28	AgCuIrPt	none	5,000	5,000	1,830	32
AgCuNbPd	none	3,860	1,640	1,790	50	AgCuNiPd	none	1,480	1,100	1,480	12	AgCuNiPt	none	3,380	1,260	1,620	13
AgCuNiSi	none	5,000	5,000	1,500	41	AgCuPdPt	fcc	1,380	760	1,590	13	AgCuPdRe	none	5,000	5,000	1,970	44
AgCuPdRh	none	3,460	1,260	1,660	17	AgCuPdRu	none	5,000	5,000	1,750	33	AgCuPtRe	none	5,000	5,000	2,020	48

	S.S.	T_c	$\tilde{T}_c$	$\bar{T}_m$	CV		S.S.	T_c	$\tilde{T}_c$	$\bar{T}_m$	CV		S.S.	T_c	$\tilde{T}_c$	$\bar{T}_m$	CV
AgCuPtRh	none	2,900	1,260	1,720	21	AgCuPtRu	none	5,000	5,000	1,800	42	AgFeIrNi	none	5,000	5,000	1,860	45
AgFeIrRu	none	5,000	5,000	2,080	50	AgFeMoNi	none	5,000	5,000	1,910	42	AgFeMoOs	fcc	1,320	3,240	2,310	48
AgFeMoPd	fcc	720	2,180	1,940	43	AgFeMoRe	fcc	1,440	3,220	2,350	41	AgFeMoRh	none	5,000	5,000	2,040	50
AgFeMoRu	none	5,000	5,000	2,130	47	AgFeNiOs	none	5,000	5,000	2,020	44	AgFeNiPd	fcc	700	1,740	1,650	41
AgFeNiRe	none	5,000	5,000	2,060	42	AgFeNiRh	none	5,000	5,000	1,750	41	AgFeNiRu	none	5,000	5,000	1,840	40
AgFeOsPd	none	5,000	5,000	2,050	45	AgFeOsRe	fcc	1,360	3,480	2,450	47	AgFeOsRh	none	5,000	5,000	2,150	50
AgFeOsRu	fcc	1,360	3,160	2,240	48	AgFePdRe	none	5,000	5,000	2,080	44	AgFePdRh	fcc	720	1,720	1,780	47
AgFePdRu	none	5,000	5,000	1,860	41	AgFeReRu	fcc	1,280	3,200	2,270	46	AgFeRhRu	none	5,000	5,000	1,970	50
AgIrMoNi	none	5,000	5,000	2,130	42	AgIrMoPd	none	5,000	5,000	2,160	41	AgIrMoRh	none	5,000	5,000	2,260	47
AgIrNbPt	none	5,000	5,000	2,180	50	AgIrNiPd	fcc	1,240	1,900	1,870	26	AgIrNiPt	fcc	1,620	1,700	1,920	24
AgIrOsPd	fcc	440	2,860	2,270	47	AgIrOsPt	none	5,000	5,000	2,320	47	AgIrPdPt	none	5,000	5,000	1,950	21
AgIrPdRe	none	5,000	5,000	2,300	41	AgIrPdRh	none	5,000	5,000	2,000	21	AgIrPdRu	fcc	420	2,460	2,080	32
AgIrPtRe	fcc	1,040	3,040	2,350	42	AgIrPtRh	fcc	380	1,500	2,050	21	AgIrPtRu	fcc	1,240	2,080	2,140	41
AgMoNiOs	none	5,000	5,000	2,290	50	AgMoNiPd	none	5,000	5,000	1,920	39	AgMoNiPt	none	5,000	5,000	1,970	42
AgMoNiRe	none	5,000	5,000	2,330	45	AgMoNiRh	none	5,000	5,000	2,020	37	AgMoNiRu	fcc	780	2,840	2,110	41
AgMoOsPd	none	5,000	5,000	2,320	47	AgMoOsRe	fcc	1,600	3,580	2,720	50	AgMoOsRh	none	5,000	5,000	2,420	50
AgMoPdPt	none	5,000	5,000	2,000	40	AgMoPdRe	fcc	1,740	2,700	2,350	42	AgMoPdRh	none	5,000	5,000	2,050	35
AgMoPdRu	none	5,000	5,000	2,130	40	AgMoPtRe	none	5,000	5,000	2,410	49	AgMoPtRh	none	5,000	5,000	2,100	50
AgMoPtRu	none	5,000	5,000	2,190	50	AgMoReRh	none	5,000	5,000	2,450	42	AgMoRhRu	none	5,000	5,000	2,240	45
AgNbPdPt	none	5,000	5,000	1,960	50	AgNbPdRh	none	5,000	5,000	2,010	49	AgNbPtRh	none	5,000	5,000	2,070	48
AgNiOsPd	fcc	460	2,640	2,030	50	AgNiOsPt	none	5,000	5,000	2,080	42	AgNiPdPt	fcc	1,580	1,080	1,700	12
AgNiPdRe	fcc	1,960	2,580	2,060	40	AgNiPdRh	fcc	720	1,360	1,760	14	AgNiPdRu	none	5,000	5,000	1,840	28
AgNiPtRe	fcc	920	2,220	2,110	44	AgNiPtRh	fcc	1,200	1,320	1,810	15	AgNiPtRu	fcc	560	1,840	1,900	33
AgOsPdPt	none	5,000	5,000	2,110	36	AgOsPdRe	fcc	960	3,560	2,460	47	AgOsPdRh	fcc	480	2,480	2,150	50
AgOsPdRu	fcc	740	3,180	2,240	42	AgOsPtRe	fcc	760	3,080	2,510	48	AgOsPtRh	fcc	1,380	2,120	2,210	50
AgOsPtRu	fcc	760	2,720	2,300	49	AgPdPtRe	fcc	1,720	2,120	2,140	40	AgPdPtRh	none	5,000	5,000	1,840	10
AgPdPtRu	fcc	1,140	1,640	1,920	26	AgPdReRh	fcc	720	2,740	2,190	36	AgPdReRu	none	5,000	5,000	2,270	40
AgPdRhRu	fcc	540	2,020	1,970	29	AgPtReRh	fcc	1,140	2,300	2,240	38	AgPtReRu	fcc	540	2,500	2,330	42
AgPtRhRu	fcc	820	1,720	2,030	28	AlCoCrCu	none	3,960	2,380	1,630	49	AlCrCuFe	none	3,680	1,860	1,600	49
AlCrFeMn	none	2,000	1,200	1,620	42	AlCrFeMo	none	2,180	1,340	1,870	50	AlCrFeNi	none	3,820	1,880	1,700	50
AlCrFeRe	none	2,080	1,400	2,080	49	AlCrFeTi	none	3,160	1,720	1,660	50	AlCrFeV	none	3,120	2,040	1,790	45
AlCrFeW	none	2,980	1,520	1,890	50	AlCrHfTi	bcc	1,740	1,300	1,860	50	AlCrHfW	none	2,320	1,900	2,160	50
AlCrMnMo	none	1,920	1,060	1,790	47	AlCrMnRe	none	2,080	1,500	1,860	43	AlCrMnTi	none	2,300	1,540	1,610	48
AlCrMnV	none	2,540	1,220	1,770	44	AlCrMnW	none	4,260	1,960	2,070	48	AlCrMoRe	bcc	1,260	1,240	2,220	45
AlCrMoTi	bcc	1,860	1,240	1,920	50	AlCrMoV	bcc	1,260	880	2,050	46	AlCrMoW	bcc	1,500	960	2,250	45
AlCrNbV	none	2,180	1,160	1,940	48	AlCrReTi	none	2,660	1,800	2,020	50	AlCrReV	bcc	1,600	1,340	2,180	48
AlCrReW	bcc	2,140	1,340	2,340	42	AlCrTiV	none	2,080	1,380	1,830	45	AlCrTiW	bcc	1,860	1,260	1,960	48
AlCrVW	bcc	1,440	880	2,120	41	AlCuFeMn	none	2,460	1,420	1,430	50	AlCuFeNi	bcc	1,380	1,440	1,580	50
AlCuFeV	none	3,900	1,860	1,720	50	AlFeMnRe	none	2,320	1,460	1,930	50	AlFeMnTi	none	4,040	2,980	1,570	50
AlFeMnV	none	3,620	1,800	1,690	47	AlFeTiV	none	2,700	1,260	1,740	50	AlHfTiV	bcc	1,660	1,160	1,900	50
AlHfTiW	bcc	1,380	1,700	2,120	50	AlHfVW	none	2,200	1,820	2,170	50	AlMnMoRe	none	2,300	1,540	1,970	50
AlMnReW	none	2,640	1,700	2,400	49	AlMnTiV	bcc	1,280	1,260	1,730	50	AlMnVW	none	2,680	1,360	2,070	48
AlMoTiV	bcc	1,280	1,060	2,040	50	AlMoVW	bcc	1,100	760	2,340	49	AlNbTiV	bcc	1,260	1,060	1,970	50
AlNbVW	bcc	580	740	2,240	50	AlReVW	bcc	1,720	1,360	2,410	50	AlTiVW	bcc	1,760	1,080	2,050	46
AuCoCrPd	fcc	720	1,820	1,770	48	AuCoCrPt	none	5,000	5,000	1,820	45	AuCoCuPd	none	4,700	1,380	1,500	18
AuCoCuPt	none	1,840	1,300	1,560	19	AuCoIrPd	fcc	640	1,760	1,900	22	AuCoIrPt	none	2,360	1,740	1,960	22
AuCoMoPd	fcc	1,200	1,860	1,960	35	AuCoMoPt	none	5,000	5,000	2,010	40	AuCoNiPd	fcc	520	1,380	1,530	26
AuCoNiPt	none	4,200	1,380	1,580	25	AuCoOsPd	none	5,000	5,000	2,060	39	AuCoOsPt	none	5,000	5,000	2,120	35
AuCoPdPt	none	1,940	1,220	1,640	13	AuCoPdRe	none	5,000	5,000	2,100	38	AuCoPdRh	none	3,900	1,340	1,790	20
AuCoPdRu	none	5,000	5,000	1,880	35	AuCoPtRe	none	5,000	5,000	2,150	35	AuCoPtRh	none	4,220	1,260	1,850	16
AuCoPtRu	none	5,000	5,000	1,930	28	AuCrCuPd	none	4,080	1,540	1,660	49	AuCrCuPt	none	5,000	5,000	1,720	47
AuCrIrPd	none	5,000	5,000	1,990	48	AuCrIrPt	none	5,000	5,000	2,050	42	AuCrNiPd	none	3,280	1,560	1,760	46
AuCrNiPt	none	5,000	5,000	1,810	42	AuCrOsPt	none	5,000	5,000	2,210	50	AuCrPdPt	fcc	560	1,740	1,830	47

	S.S.	T_c	$\tilde{T}_c$	$\bar{T}_m$	CV		S.S.	T_c	$\tilde{T}_c$	$\bar{T}_m$	CV		S.S.	T_c	$\tilde{T}_c$	$\bar{T}_m$	CV
AuCrPdRh	none	5,000	5,000	1,880	46	AuCrPdRu	none	5,000	5,000	1,970	50	AuCrPtRh	none	5,000	5,000	1,940	40
AuCrPtRu	none	5,000	5,000	2,020	46	AuCuFePd	fcc	1,320	900	1,580	40	AuCuIrPd	none	5,000	5,000	1,800	27
AuCuIrPt	none	5,000	5,000	1,860	24	AuCuNiPd	none	2,140	880	1,450	14	AuCuNiPt	none	2,300	1,020	1,500	14
AuCuOsPt	none	5,000	5,000	2,010	47	AuCuPdPt	none	1,620	780	1,580	10	AuCuPdRe	fcc	460	2,180	1,990	50
AuCuPdRh	none	3,820	1,120	1,690	15	AuCuPdRu	fcc	500	1,880	1,780	43	AuCuPtRe	fcc	760	2,440	2,050	46
AuCuPtRh	none	1,960	1,040	1,740	16	AuCuPtRu	fcc	1,520	1,680	1,830	33	AuFeMoPd	none	2,280	1,580	1,970	49
AuFeNiPd	fcc	940	1,160	1,670	48	AuFeOsPd	none	5,000	5,000	2,070	50	AuFePdRe	fcc	540	2,100	2,110	48
AuFePdRh	none	5,000	5,000	1,800	50	AuFePdRu	none	5,000	5,000	1,890	46	AuIrMoPd	none	5,000	5,000	2,180	37
AuIrNiPd	fcc	980	1,760	1,890	24	AuIrNiPt	none	2,060	1,560	1,950	23	AuIrOsPd	fcc	500	2,760	2,290	45
AuIrOsPt	fcc	940	2,220	2,350	40	AuIrPdPt	fcc	340	1,500	1,970	19	AuIrPdRe	none	5,000	5,000	2,330	38
AuIrPdRh	fcc	540	1,760	2,020	19	AuIrPdRu	fcc	800	2,360	2,110	35	AuIrPtRe	none	5,000	5,000	2,380	39
AuIrPtRh	fcc	380	1,320	2,080	19	AuIrPtRu	fcc	1,420	1,880	2,160	26	AuMoNiPd	fcc	660	1,660	1,950	37
AuMoNiPt	none	5,000	5,000	2,000	42	AuMoOsPd	none	5,000	5,000	2,340	44	AuMoPdPt	none	5,000	5,000	2,020	39
AuMoPdRe	fcc	1,440	2,160	2,380	38	AuMoPdRh	none	5,000	5,000	2,070	32	AuMoPdRu	fcc	1,260	2,020	2,160	36
AuMoPtRe	none	5,000	5,000	2,430	44	AuMoPtRh	fcc	340	1,920	2,130	50	AuMoPtRu	none	5,000	5,000	2,210	39
AuNbPdRh	none	2,100	1,920	2,040	50	AuNbPtRh	none	5,000	5,000	2,090	50	AuNiOsPd	fcc	560	2,340	2,050	49
AuNiOsPt	none	5,000	5,000	2,110	38	AuNiPdPt	none	2,700	1,080	1,600	12	AuNiPdRe	none	2,140	2,260	2,090	34
AuNiPdRh	none	3,400	1,160	1,780	13	AuNiPdRu	fcc	620	1,800	1,870	32	AuNiPtRe	fcc	2,100	2,060	2,140	37
AuNiPtRh	none	3,320	1,100	1,840	14	AuNiPtRu	none	3,220	1,520	1,920	26	AuOsPdPt	fcc	1,060	2,120	2,130	36
AuOsPdRe	fcc	1,020	3,300	2,480	46	AuOsPdRh	fcc	780	2,300	2,180	48	AuOsPtRh	fcc	1,080	1,900	2,230	45
AuOsPtRu	none	5,000	5,000	2,320	37	AuPdPtRe	fcc	460	2,160	2,170	43	AuPdPtRh	none	3,060	940	1,860	9
AuPdPtRu	fcc	1,680	1,640	1,950	22	AuPdReRh	fcc	900	2,500	2,210	32	AuPdReRu	fcc	980	2,720	2,300	37
AuPdRhRu	fcc	940	1,800	2,000	22	AuPtReRh	none	5,000	5,000	2,270	38	AuPtReRu	fcc	1,300	2,320	2,350	35
AuPtRhRu	fcc	600	1,440	2,050	23	CoCrCuNi	none	2,340	1,400	1,670	48	CoCrCuPd	none	4,280	1,680	1,620	34
CoCrCuPt	none	3,360	1,420	1,780	34	CoCrFeNi	fcc	1,600	1,000	1,720	47	CoCrIrPd	none	4,260	1,680	1,790	33
CoCrIrPt	none	2,020	1,520	1,950	31	CoCrMnMo	none	1,860	1,260	1,780	50	CoCrMnNb	none	1,920	1,300	1,680	50
CoCrMnNi	fcc	1,280	1,020	1,580	37	CoCrMoNb	bcc	1,740	1,320	2,040	43	CoCrMoW	bcc	1,640	1,340	2,390	44
CoCrNbW	bcc	1,760	1,380	2,250	43	CoCrNiPd	none	3,080	1,140	1,600	33	CoCrNiPt	none	3,160	1,220	1,750	32
CoCrOsPd	none	2,660	1,780	2,260	34	CoCrOsPt	none	2,560	1,500	2,320	33	CoCrPdPt	none	3,200	1,320	1,720	35
CoCrPdRh	none	3,080	1,340	1,700	37	CoCrPdRu	none	2,900	1,340	2,080	34	CoCrPtRh	none	1,900	1,180	1,850	32
CoCrPtRu	fcc	1,860	1,300	2,130	32	CoCuIrPd	none	4,380	1,400	1,740	26	CoCuIrPt	none	3,360	1,240	1,880	25
CoCuNiPd	none	2,900	980	1,570	22	CoCuNiPt	fcc	840	840	1,700	18	CoCuOsPd	none	5,000	5,000	2,070	40
CoCuOsPt	none	3,320	1,920	2,120	32	CoCuPdPt	fcc	1,640	960	1,670	18	CoCuPdRe	fcc	1,440	2,040	2,100	34
CoCuPdRh	none	2,820	1,220	1,630	28	CoCuPdRu	none	3,780	1,840	1,880	36	CoCuPtRe	fcc	960	1,660	2,160	35
CoCuPtRh	fcc	1,560	960	1,770	20	CoCuPtRu	none	3,320	1,460	1,940	27	CoFeMnNi	fcc	1,550	900	1,600	48
CoIrMoPd	none	3,640	1,680	1,930	32	CoIrMoPt	none	2,460	1,460	2,090	34	CoIrNiPd	none	2,340	820	1,780	23
CoIrNiPt	none	2,100	800	1,910	26	CoIrOsPd	fcc	580	1,260	2,400	20	CoIrOsPt	fcc	2,380	1,180	2,450	16
CoIrPdPt	none	1,980	940	1,850	18	CoIrPdRe	fcc	2,000	1,640	2,430	25	CoIrPdRh	none	2,260	800	1,900	19
CoIrPdRu	none	2,300	1,220	2,220	19	CoIrPtRe	fcc	2,440	1,620	2,490	28	CoIrPtRh	fcc	1,820	720	2,040	17
CoIrPtRu	none	2,460	1,040	2,270	15	CoMoNbW	bcc	2,000	1,340	2,550	47	CoMoNiPd	none	2,100	1,220	1,760	39
CoMoNiPt	none	2,180	1,100	1,910	40	CoMoOsPd	none	2,820	1,740	2,450	31	CoMoOsPt	fcc	1,180	1,760	2,510	33
CoMoPdPt	none	1,960	1,280	1,900	38	CoMoPdRe	fcc	2,300	1,660	2,480	31	CoMoPdRh	none	2,680	1,360	1,880	34
CoMoPdRu	none	2,500	1,560	2,270	31	CoMoPtRe	fcc	1,740	1,840	2,540	35	CoMoPtRh	fcc	1,980	1,180	2,030	34
CoMoPtRu	fcc	2,240	1,400	2,320	32	CoNiOsPd	none	2,820	1,300	2,160	26	CoNiOsPt	none	2,280	1,140	2,210	30
CoNiPdPt	none	1,800	700	1,680	24	CoNiPdRe	fcc	1,980	1,180	2,190	28	CoNiPdRh	none	2,320	800	1,690	25
CoNiPdRu	none	3,540	1,140	1,980	24	CoNiPtRe	fcc	1,620	900	2,250	30	CoNiPtRh	fcc	1,720	660	1,820	20
CoNiPtRu	none	2,120	860	2,030	20	CoOsPdPt	none	2,660	1,480	2,240	25	CoOsPdRe	fcc	1,220	1,760	2,590	24
CoOsPdRh	fcc	1,920	1,280	2,290	24	CoOsPdRu	fcc	1,880	1,660	2,370	21	CoOsPtRe	fcc	900	1,460	2,650	23
CoOsPtRh	fcc	1,780	1,100	2,340	21	CoOsPtRu	fcc	2,340	1,420	2,430	17	CoPdPtRe	fcc	1,000	1,140	2,270	27
CoPdPtRh	fcc	1,600	740	1,810	18	CoPdPtRu	fcc	1,040	1,020	2,060	20	CoPdReRh	none	2,320	1,420	2,320	27
CoPdReRu	fcc	1,400	1,580	2,410	24	CoPdRhRu	none	2,220	1,100	2,100	24	CoPtReRh	fcc	980	1,000	2,380	26
CoPtReRu	fcc	1,420	900	2,460	22	CoPtRhRu	fcc	1,400	840	2,160	15	CrCuFeMn	none	5,000	5,000	1,640	50
CrCuFeMo	none	4,500	1,900	1,840	48	CrCuFeNb	none	3,660	1,840	1,850	47	CrCuFeNi	none	3,360	1,560	1,700	50

	S.S.	T_c	$\tilde{T}_c$	$\bar{T}_m$	CV		S.S.	T_c	$\tilde{T}_c$	$\bar{T}_m$	CV		S.S.	T_c	$\tilde{T}_c$	$\bar{T}_m$	CV
CrCuFePd	none	5,000	5,000	1,660	41	CrCuFeV	none	4,920	1,800	1,910	36	CrCuFeW	none	4,820	2,140	2,060	48
CrCuIrPd	none	5,000	5,000	1,860	38	CrCuIrPt	none	5,000	5,000	2,020	37	CrCuMnV	none	5,000	5,000	1,800	47
CrCuMnW	none	5,000	5,000	2,170	50	CrCuMoTa	none	5,000	5,000	2,010	45	CrCuMoTi	none	3,380	1,920	1,780	50
CrCuMoV	none	5,000	5,000	2,040	47	CrCuMoW	none	5,000	5,000	2,290	50	CrCuNbTa	none	3,560	1,980	2,050	48
CrCuNbTi	none	2,740	1,860	1,800	50	CrCuNbV	none	3,520	1,700	2,050	44	CrCuNbW	none	5,000	5,000	2,290	46
CrCuNiPd	none	3,320	1,380	1,590	31	CrCuNiPt	none	3,240	1,360	1,740	30	CrCuOsPd	fcc	760	2,240	2,160	46
CrCuOsPt	fcc	480	2,080	2,210	45	CrCuPdPt	none	4,000	1,460	1,740	38	CrCuPdRh	none	4,640	1,600	1,700	36
CrCuPdRu	none	5,000	5,000	1,970	40	CrCuPtRh	none	2,680	1,580	1,860	35	CrCuPtRu	none	3,680	1,680	2,030	40
CrCuTaTi	none	2,840	2,100	1,810	48	CrCuTaV	none	3,820	2,080	2,030	41	CrCuTaW	none	5,000	5,000	2,330	44
CrCuTiV	none	3,460	1,820	1,830	42	CrCuTiW	none	4,140	2,100	2,010	50	CrCuVW	none	5,000	5,000	2,300	42
CrFeMnMo	none	2,160	1,080	1,870	26	CrFeMnNb	none	2,760	1,300	1,760	27	CrFeMnNi	none	1,620	1,160	1,620	50
CrFeMnRe	bcc	1,120	1,220	2,230	31	CrFeMnTa	none	3,680	1,580	1,850	28	CrFeMnTi	none	5,000	5,000	1,640	39
CrFeMnV	bcc	1,720	1,000	1,800	21	CrFeMnW	bcc	2,100	1,180	2,280	38	CrFeMoNb	none	2,360	1,360	2,140	27
CrFeMoNi	bcc	1,560	1,140	1,910	50	CrFeMoRe	bcc	1,740	1,040	2,570	28	CrFeMoTa	none	3,140	1,840	2,250	30
CrFeMoTi	none	3,540	1,780	1,950	30	CrFeMoV	bcc	1,820	940	2,080	23	CrFeMoW	bcc	2,220	1,220	2,310	34
CrFeNbRe	none	2,600	1,520	2,530	34	CrFeNbTa	none	3,280	1,600	2,150	26	CrFeNbTi	none	4,420	2,140	1,840	34
CrFeNbV	none	2,520	1,320	1,950	22	CrFeNbW	bcc	2,160	1,320	2,170	33	CrFeNiPd	none	2,620	1,320	1,640	50
CrFeNiRe	bcc	1,560	1,020	2,280	50	CrFeNiV	bcc	1,420	800	1,740	49	CrFeOsPd	fcc	1,900	1,860	2,270	44
CrFePdRu	fcc	1,880	1,760	2,090	43	CrFeReTa	none	3,660	1,860	2,670	33	CrFeReTi	none	3,060	1,580	2,330	38
CrFeReV	bcc	2,000	1,160	2,390	29	CrFeReW	bcc	2,120	1,100	2,770	38	CrFeTaTi	none	4,160	2,080	1,980	36
CrFeTaV	none	3,120	1,540	2,060	25	CrFeTaW	none	3,000	1,520	2,350	40	CrFeTiV	none	3,960	1,840	1,800	29
CrFeTiW	none	3,660	1,840	1,970	36	CrFeVW	bcc	1,880	1,000	2,120	28	CrHfMoNb	bcc	2,240	1,600	2,290	24
CrHfMoRe	none	2,560	1,740	2,420	31	CrHfMoTa	bcc	2,120	1,880	2,360	24	CrHfMoTi	bcc	1,960	1,540	2,060	31
CrHfMoV	none	2,600	1,560	2,130	28	CrHfMoW	bcc	2,120	1,760	2,500	25	CrHfMoZr	bcc	1,880	2,080	2,030	34
CrHfNbRe	none	2,760	2,060	2,400	32	CrHfNbTa	bcc	1,300	1,520	2,360	22	CrHfNbTi	bcc	1,280	1,420	2,040	27
CrHfNbV	none	2,600	1,660	2,080	26	CrHfNbW	bcc	1,660	1,700	2,450	23	CrHfNbZr	bcc	1,460	1,840	2,060	30
CrHfReTa	none	4,060	2,320	2,500	34	CrHfReTi	none	2,600	1,840	2,210	36	CrHfReV	none	3,260	1,960	2,300	34
CrHfReW	none	3,180	1,820	2,640	32	CrHfReZr	none	2,260	2,340	2,180	41	CrHfTaTi	bcc	1,260	1,580	2,150	28
CrHfTaV	bcc	1,800	2,000	2,160	26	CrHfTaW	bcc	1,660	1,880	2,590	23	CrHfTaZr	bcc	2,040	2,060	2,130	31
CrHfTiV	bcc	1,720	1,500	1,900	31	CrHfTiW	bcc	1,360	1,680	2,210	29	CrHfTiZr	bcc	1,820	1,840	1,890	36
CrHfVW	none	2,620	1,600	2,300	50	CrHfVZr	none	3,480	1,940	1,880	37	CrHfWZr	bcc	2,120	2,460	2,390	32
CrIrNiPd	none	3,760	1,540	1,850	32	CrIrNiPt	none	2,760	1,480	2,000	30	CrIrOsPd	none	3,860	1,740	2,490	34
CrIrOsPt	fcc	1,880	1,360	2,540	30	CrIrPdPt	none	3,140	1,760	1,980	33	CrIrPdRh	fcc	1,440	1,500	2,030	32
CrIrPdRu	none	3,400	1,620	2,310	32	CrIrPtRh	fcc	1,660	1,160	2,190	26	CrIrPtRu	fcc	1,540	1,220	2,360	29
CrMnMoNb	none	2,640	1,360	2,030	20	CrMnMoNi	none	1,960	1,280	1,770	50	CrMnMoRe	bcc	1,560	1,240	2,120	20
CrMnMoTa	none	3,500	1,760	2,100	19	CrMnMoTi	none	2,520	1,400	1,860	23	CrMnMoV	none	2,280	1,200	2,010	16
CrMnMoW	bcc	1,880	1,260	2,560	17	CrMnMoZr	none	5,000	5,000	1,750	45	CrMnNbNi	none	2,760	1,480	1,620	50
CrMnNbRe	none	3,160	1,400	2,030	25	CrMnNbTa	none	4,380	1,720	2,030	24	CrMnNbTi	none	3,240	1,640	1,760	27
CrMnNbV	none	3,020	1,520	1,900	18	CrMnNbW	none	2,600	1,340	2,520	21	CrMnNbZr	none	2,680	1,900	1,720	42
CrMnNiRe	bcc	1,700	1,240	1,780	50	CrMnNiV	none	2,060	1,180	1,660	49	CrMnReTa	none	4,040	1,680	2,130	28
CrMnReTi	none	1,900	1,320	1,890	29	CrMnReV	bcc	1,440	800	2,080	21	CrMnReW	bcc	1,780	1,380	2,700	22
CrMnReZr	none	2,600	2,020	1,800	47	CrMnTaTi	none	4,060	1,900	1,870	28	CrMnTaV	none	4,100	1,960	1,980	18
CrMnTaW	none	3,580	1,840	2,650	21	CrMnTaZr	none	3,800	2,340	1,780	44	CrMnTiV	none	2,640	1,300	1,770	23
CrMnTiW	none	3,380	1,540	2,320	25	CrMnTiZr	none	3,060	1,920	1,600	47	CrMnVW	bcc	2,240	1,180	2,370	17
CrMnWZr	none	3,640	3,060	2,360	46	CrMoNbNi	none	2,200	1,280	2,040	50	CrMoNbRe	bcc	2,360	1,180	2,510	13
CrMoNbTa	bcc	2,500	1,100	2,550	10	CrMoNbTi	bcc	1,860	1,120	2,200	14	CrMoNbV	bcc	2,220	1,000	2,300	6
CrMoNbW	none	2,880	920	2,630	6	CrMoNbZr	none	2,940	1,980	2,090	21	CrMoNiRe	bcc	1,580	960	2,180	50
CrMoReTa	none	3,040	1,660	2,630	17	CrMoReTi	bcc	1,960	1,420	2,310	23	CrMoReV	bcc	1,140	940	2,470	11
CrMoReW	bcc	1,340	740	2,760	8	CrMoReZr	none	2,500	1,500	2,160	29	CrMoTaTi	bcc	1,600	1,340	2,320	15
CrMoTaV	bcc	2,040	1,140	2,400	6	CrMoTaW	bcc	2,620	1,040	2,790	7	CrMoTaZr	none	3,220	2,180	2,180	37
CrMoTiV	bcc	1,580	920	2,110	14	CrMoTiW	bcc	1,820	960	2,370	15	CrMoTiZr	none	2,140	1,520	1,910	28
CrMoVW	bcc	1,500	660	2,530	5	CrMoVZr	none	3,640	3,100	1,970	25	CrMoWZr	none	4,100	2,780	2,430	22
CrNbNiV	none	2,240	1,380	1,810	47	CrNbReTa	none	3,280	1,600	2,560	19	CrNbReTi	bcc	2,200	1,520	2,220	24

	S.S.	T_c	$\tilde{T}_c$	$\bar{T}_m$	CV		S.S.	T_c	$\tilde{T}_c$	$\bar{T}_m$	CV		S.S.	T_c	$\tilde{T}_c$	$\bar{T}_m$	CV
CrNbReV	none	2,380	1,340	2,350	16	CrNbReW	bcc	2,160	1,240	2,640	14	CrNbReZr	none	2,680	2,020	2,120	30
CrNbTaTi	bcc	1,340	1,080	2,250	13	CrNbTaV	bcc	2,280	1,020	2,300	7	CrNbTaW	bcc	2,340	840	2,680	7
CrNbTaZr	none	2,380	2,240	2,160	19	CrNbTiV	bcc	1,820	1,100	1,990	13	CrNbTiW	bcc	1,660	1,040	2,250	14
CrNbTiZr	none	3,900	2,220	1,880	24	CrNbVW	bcc	1,980	880	2,380	7	CrNbVZr	none	4,400	3,360	1,910	23
CrNbWZr	none	4,600	3,240	2,360	20	CrNiOsPd	fcc	1,600	1,560	2,250	34	CrNiOsPt	none	3,040	1,540	2,300	33
CrNiPdPt	none	3,960	1,460	1,710	31	CrNiPdRh	none	3,080	1,340	1,720	32	CrNiPdRu	none	2,560	1,440	2,070	31
CrNiPtRh	none	3,160	1,300	1,860	30	CrNiPtRu	none	2,600	1,240	2,120	31	CrNiReV	bcc	1,700	1,200	2,050	50
CrOsPdPt	none	3,220	1,900	2,330	36	CrOsPdRh	none	2,540	1,600	2,380	34	CrOsPdRu	none	2,980	1,740	2,460	34
CrOsPtRh	fcc	1,340	1,420	2,430	31	CrOsPtRu	none	2,540	1,480	2,520	31	CrPdPtRh	none	2,280	1,420	1,890	33
CrPdPtRu	none	2,980	1,560	2,150	35	CrPdRhRu	none	2,720	1,240	2,190	33	CrPtRhRu	fcc	1,800	960	2,250	30
CrReTaTi	none	2,880	1,800	2,370	26	CrReTaV	none	2,960	1,580	2,480	18	CrReTaW	none	2,920	1,500	2,830	17
CrReTaZr	none	3,600	2,280	2,240	32	CrReTiV	bcc	1,680	1,260	2,190	23	CrReTiW	none	2,440	1,520	2,420	24
CrReTiZr	none	2,280	1,820	1,980	34	CrReVW	bcc	1,180	980	2,600	12	CrReVZr	none	3,260	2,020	2,060	33
CrReWZr	none	2,580	1,800	2,480	29	CrTaTiV	bcc	1,780	1,380	2,120	14	CrTaTiW	bcc	1,320	1,200	2,440	14
CrTaTiZr	none	3,400	2,340	1,990	24	CrTaVW	bcc	1,460	960	2,550	7	CrTaVZr	none	4,080	3,220	2,000	24
CrTaWZr	none	4,180	3,040	2,510	21	CrTiVW	bcc	1,220	780	2,170	13	CrTiVZr	none	3,000	1,600	1,770	28
CrTiWZr	none	2,740	1,760	2,160	26	CrVWZr	none	4,900	1,740	2,240	26	CuFeIrPd	none	2,140	1,300	1,920	47
CuFeMnNb	none	3,400	1,860	1,670	50	CuFeMnTa	none	4,620	2,540	1,600	50	CuFeMnTi	none	3,720	2,080	1,470	50
CuFeMnV	none	4,800	2,000	1,730	45	CuFeMoTi	none	3,160	1,900	1,710	50	CuFeMoV	none	3,900	1,560	1,940	45
CuFeNbTa	none	3,340	1,740	1,990	50	CuFeNbTi	none	3,740	1,740	1,760	49	CuFeNbV	none	3,020	1,680	1,970	44
CuFeNiPd	none	1,880	920	1,590	38	CuFeNiV	none	2,600	1,060	1,740	47	CuFeOsPd	fcc	740	1,860	2,080	41
CuFePdRe	fcc	1,160	1,740	2,110	41	CuFePdRh	none	2,360	1,020	1,810	44	CuFePdRu	none	4,240	1,560	1,890	33
CuFeTaV	none	3,380	1,800	1,930	43	CuFeTiV	none	3,420	1,780	1,750	41	CuFeVW	none	4,600	1,860	2,130	48
CuIrNiPd	none	3,200	1,160	1,780	19	CuIrNiPt	none	2,860	1,000	1,920	19	CuIrOsPd	fcc	480	2,020	2,300	37
CuIrOsPt	none	5,000	5,000	2,350	41	CuIrPdPt	none	4,060	1,120	1,890	20	CuIrPdRe	none	5,000	5,000	2,330	49
CuIrPdRh	none	3,760	1,200	1,920	20	CuIrPdRu	none	5,000	5,000	2,110	38	CuIrPtRe	none	5,000	5,000	2,380	38
CuIrPtRh	none	2,360	1,100	2,070	23	CuIrPtRu	none	5,000	5,000	2,170	31	CuMnMoTa	none	4,680	2,240	1,720	50
CuMnMoV	none	4,800	1,900	1,810	48	CuMnMoW	none	4,800	2,180	2,360	50	CuMnNbTa	none	4,360	2,140	1,800	50
CuMnNbV	none	3,980	2,020	1,850	50	CuMnTaV	none	4,540	2,240	1,780	47	CuMnTaW	none	5,000	5,000	2,460	50
CuMnTiV	none	3,520	2,020	1,650	50	CuMnVW	none	5,000	5,000	2,180	50	CuMoNbTa	none	4,400	1,520	2,250	49
CuMoNbV	none	3,700	1,460	2,190	47	CuMoNbW	none	5,000	5,000	2,480	50	CuMoTaTi	none	3,160	1,740	1,950	50
CuMoTaW	none	5,000	5,000	2,480	47	CuMoTiV	none	2,900	1,520	1,920	46	CuMoVW	none	5,000	5,000	2,400	50
CuNbPdPt	none	5,000	5,000	1,990	50	CuNbPdRh	fcc	900	2,040	2,040	50	CuNbPtRh	none	5,000	5,000	2,100	50
CuNbTaTi	none	2,300	1,280	2,030	50	CuNbTaV	none	2,300	1,520	2,190	45	CuNbTaW	none	5,000	5,000	2,530	48
CuNbTiV	bcc	1,860	1,480	1,960	47	CuNbVW	none	4,360	1,600	2,410	46	CuNiOsPd	fcc	1,220	1,820	2,060	34
CuNiOsPt	fcc	920	1,640	2,110	31	CuNiPdPt	fcc	1,240	680	1,640	12	CuNiPdRe	fcc	1,880	1,840	2,090	36
CuNiPdRh	none	2,360	840	1,640	12	CuNiPdRu	none	3,700	1,480	1,870	22	CuNiPtRe	fcc	1,640	1,540	2,150	36
CuNiPtRh	fcc	1,640	840	1,760	13	CuNiPtRu	fcc	1,160	1,180	1,930	22	CuOsPdPt	fcc	360	1,680	2,140	35
CuOsPdRe	none	5,000	5,000	2,490	50	CuOsPdRh	none	5,000	5,000	2,190	41	CuOsPdRu	none	5,000	5,000	2,270	50
CuOsPtRe	fcc	980	2,360	2,540	42	CuOsPtRh	fcc	1,880	1,640	2,240	37	CuOsPtRu	fcc	1,320	2,100	2,330	35
CuPdPtRe	fcc	900	1,660	2,170	39	CuPdPtRh	none	1,980	780	1,790	14	CuPdPtRu	fcc	280	1,160	1,950	24
CuPdReRh	fcc	860	2,100	2,220	34	CuPdReRu	none	5,000	5,000	2,300	38	CuPdRhRu	fcc	420	1,500	2,000	32
CuPtReRh	fcc	780	1,680	2,270	35	CuPtReRu	fcc	880	1,880	2,360	36	CuPtRhRu	fcc	1,560	1,140	2,060	36
CuTaTiV	none	2,360	1,780	1,930	44	CuTaTiW	none	3,760	1,860	2,210	50	CuTaVW	none	4,520	1,620	2,420	50
CuTiVW	none	3,580	1,800	2,120	46	FeIrMoPd	none	4,200	1,800	2,300	50	FeIrNiPd	fcc	1,900	1,040	2,010	50
FeIrOsPd	fcc	880	1,520	2,410	43	FeIrPdRe	none	2,580	1,800	2,440	46	FeIrPdRu	fcc	640	1,420	2,230	43
FeMnMoNb	none	2,360	1,540	1,980	31	FeMnMoRe	bcc	2,300	1,220	2,420	35	FeMnMoTa	none	3,140	1,620	2,030	34
FeMnMoTi	none	3,280	1,580	1,800	32	FeMnMoV	none	1,960	1,060	1,920	25	FeMnMoW	none	2,700	1,560	2,470	42
FeMnNbRe	none	2,960	1,480	2,380	39	FeMnNbTa	none	4,360	1,860	1,980	31	FeMnNbTi	none	4,500	2,240	1,730	41
FeMnNbV	none	2,720	1,640	1,830	26	FeMnNbW	none	2,460	1,420	2,440	39	FeMnReTa	none	4,000	1,600	2,510	38
FeMnReTi	bcc	1,040	1,280	2,180	40	FeMnReV	bcc	1,740	920	2,240	34	FeMnReW	bcc	1,740	1,520	2,620	44
FeMnTaTi	none	5,000	5,000	1,820	47	FeMnTaV	none	3,820	1,820	1,890	29	FeMnTaW	none	2,760	1,520	2,570	37
FeMnTiV	none	4,280	2,060	1,690	32	FeMnTiW	none	4,020	1,880	2,240	39	FeMnVW	bcc	2,120	1,260	2,290	30

	S.S.	T_c	$\tilde{T}_c$	$\bar{T}_m$	CV		S.S.	T_c	$\tilde{T}_c$	$\bar{T}_m$	CV		S.S.	T_c	$\tilde{T}_c$	$\bar{T}_m$	CV
FeMoNbRe	none	2,840	1,380	2,720	36	FeMoNbTa	none	3,020	1,500	2,470	30	FeMoNbTi	none	4,200	2,200	2,140	32
FeMoNbV	bcc	2,200	1,200	2,210	27	FeMoNbW	none	3,300	1,440	2,480	37	FeMoNiPd	fcc	1,780	1,160	1,810	50
FeMoNiV	none	2,120	980	1,910	50	FeMoOsPd	none	2,480	1,640	2,460	39	FeMoPdRe	fcc	2,040	1,480	2,490	37
FeMoPdRh	none	3,280	1,460	2,190	50	FeMoPdRu	fcc	2,080	1,640	2,280	39	FeMoReTa	none	3,100	1,700	2,860	37
FeMoReTi	bcc	2,240	1,600	2,520	40	FeMoReV	bcc	2,160	1,240	2,580	31	FeMoReW	bcc	2,520	1,120	2,960	41
FeMoTaTi	none	4,420	2,380	2,240	35	FeMoTaV	none	2,640	1,320	2,290	30	FeMoTaW	none	3,780	1,320	2,620	40
FeMoTiV	none	3,700	1,920	2,010	30	FeMoTiW	none	3,680	1,680	2,210	40	FeMoVW	none	2,440	1,040	2,340	35
FeNbReTa	none	4,040	1,860	2,820	38	FeNbReTi	none	4,420	2,160	2,480	43	FeNbReV	none	2,680	1,500	2,540	35
FeNbReW	none	3,080	1,480	2,920	44	FeNbTaTi	none	4,300	1,780	2,190	33	FeNbTaV	bcc	1,840	1,080	2,210	24
FeNbTaW	none	2,660	1,340	2,530	35	FeNbTiV	none	3,440	1,840	1,920	28	FeNbTiW	none	4,380	2,160	2,110	36
FeNbVW	bcc	1,920	1,120	2,210	32	FeNiOsPd	none	2,740	1,380	2,170	43	FeNiPdRe	fcc	2,100	1,260	2,200	45
FeNiPdRh	none	2,520	1,080	1,900	50	FeNiPdRu	none	3,300	1,320	1,990	42	FeOsPdRe	fcc	1,180	1,920	2,600	32
FeOsPdRh	fcc	2,040	1,440	2,300	43	FeOsPdRu	fcc	920	1,840	2,380	29	FePdReRh	none	2,460	1,600	2,330	46
FePdReRu	fcc	1,160	1,760	2,420	32	FePdRhRu	none	2,780	1,280	2,110	41	FeReTaTi	none	5,000	5,000	2,620	44
FeReTaV	none	3,560	1,700	2,670	34	FeReTiV	none	4,100	2,060	2,340	40	FeReVW	bcc	2,760	1,360	2,780	41
FeTaTiV	none	3,340	1,840	2,030	31	FeTaTiW	none	4,520	2,220	2,290	39	FeTaVW	none	2,360	1,220	2,360	34
FeTiVW	none	4,040	1,960	1,990	33	HfMoNbRe	none	2,860	1,520	2,620	28	HfMoNbTa	bcc	1,320	740	2,660	15
HfMoNbTi	bcc	1,400	860	2,330	22	HfMoNbV	bcc	1,580	1,000	2,330	19	HfMoNbW	bcc	1,580	820	2,740	17
HfMoNbZr	bcc	880	1,040	2,280	22	HfMoReTa	none	3,820	1,860	2,680	29	HfMoReTi	bcc	2,320	1,460	2,370	35
HfMoReV	none	2,640	1,620	2,430	31	HfMoReW	none	2,940	1,700	2,810	28	HfMoReZr	none	2,600	1,800	2,280	35
HfMoTaTi	bcc	1,440	960	2,390	22	HfMoTaV	bcc	1,580	1,380	2,370	20	HfMoTaW	bcc	1,760	1,200	2,840	17
HfMoTaZr	bcc	1,440	1,400	2,300	22	HfMoTiV	bcc	1,520	1,040	2,090	26	HfMoTiW	bcc	1,520	1,060	2,440	25
HfMoTiZr	bcc	1,420	940	2,050	29	HfMoVW	bcc	1,960	1,060	2,500	22	HfMoVZr	bcc	1,820	1,380	2,010	29
HfMoWZr	bcc	1,460	1,740	2,550	25	HfNbReTa	bcc	620	1,160	2,720	29	HfNbReTi	bcc	1,320	1,200	2,390	33
HfNbReV	bcc	1,720	1,380	2,430	30	HfNbReW	bcc	2,500	1,500	2,790	29	HfNbReZr	bcc	1,560	1,380	2,360	34
HfNbTaTi	bcc	1,200	700	2,430	16	HfNbTaV	bcc	1,080	1,160	2,380	13	HfNbTaW	bcc	960	920	2,850	13
HfNbTaZr	bcc	1,540	940	2,400	16	HfNbTiV	bcc	1,460	1,080	2,090	20	HfNbTiW	bcc	1,120	760	2,430	20
HfNbTiZr	bcc	980	840	2,130	22	HfNbVW	bcc	1,280	1,060	2,460	18	HfNbVZr	bcc	2,020	1,400	2,070	22
HfNbWZr	bcc	1,500	1,220	2,600	20	HfReTaTi	bcc	1,300	1,280	2,480	34	HfReTaV	bcc	1,560	1,560	2,490	31
HfReTaW	none	3,440	1,860	2,920	30	HfReTaZr	none	2,800	1,740	2,410	35	HfReTiV	bcc	1,780	1,380	2,220	35
HfReTiW	bcc	1,820	1,440	2,530	36	HfReTiZr	bcc	1,460	1,300	2,160	38	HfReVW	bcc	2,540	1,520	2,610	32
HfReVZr	none	2,520	1,860	2,150	38	HfReWZr	bcc	1,600	2,140	2,650	35	HfTaTiV	bcc	1,420	1,400	2,160	20
HfTaTiW	bcc	1,440	960	2,560	20	HfTaTiZr	bcc	1,340	1,040	2,190	22	HfTaVW	bcc	1,420	1,300	2,570	18
HfTaVZr	bcc	1,880	1,760	2,100	21	HfTaWZr	bcc	1,980	1,440	2,690	19	HfTiVW	bcc	1,660	1,100	2,200	23
HfTiVZr	none	2,640	1,400	1,880	30	HfTiWZr	bcc	1,420	1,400	2,350	26	HfVWZr	none	2,700	1,740	2,340	27
IrMoNiPd	none	3,240	1,340	2,020	34	IrMoNiPt	fcc	1,920	1,320	2,170	35	IrMoOsPd	fcc	2,660	1,520	2,680	27
IrMoOsPt	fcc	2,000	1,720	2,730	29	IrMoPdPt	fcc	2,160	1,620	2,170	33	IrMoPdRe	none	3,160	1,800	2,710	30
IrMoPdRh	none	2,600	1,440	2,210	26	IrMoPdRu	none	2,860	1,520	2,210	26	IrMoPtRe	fcc	1,080	2,020	2,770	40
IrMoPtRh	fcc	1,960	1,340	2,370	27	IrMoPtRu	fcc	2,140	1,440	2,420	28	IrNbPdPt	none	5,000	5,000	2,320	46
IrNbPdRh	fcc	260	2,920	2,370	40	IrNbPdRu	none	5,000	5,000	2,460	50	IrNbPtRh	none	5,000	5,000	2,430	40
IrNbPtRu	none	5,000	5,000	2,510	50	IrNiOsPd	fcc	1,120	1,260	2,390	20	IrNiOsPt	fcc	2,340	1,060	2,440	20
IrNiPdPt	none	1,980	860	1,910	14	IrNiPdRe	fcc	2,200	1,100	2,420	27	IrNiPdRh	fcc	1,960	800	1,990	18
IrNiPdRu	fcc	540	1,120	2,000	17	IrNiPtRe	fcc	1,600	1,520	2,480	27	IrNiPtRh	fcc	1,940	720	2,120	14
IrNiPtRu	fcc	2,140	940	2,170	17	IrOsPdPt	none	3,080	1,220	2,470	21	IrOsPdRe	none	3,900	1,720	2,820	23
IrOsPdRh	none	2,740	1,000	2,520	22	IrOsPdRu	none	4,120	1,300	2,600	19	IrOsPtRe	fcc	2,100	1,300	2,870	20
IrOsPtRh	fcc	1,300	780	2,570	16	IrOsPtRu	fcc	1,660	800	2,660	11	IrPdPtRe	fcc	1,660	1,580	2,500	27
IrPdPtRh	fcc	1,820	720	2,120	10	IrPdPtRu	none	2,960	1,000	2,160	14	IrPdReRh	none	3,020	1,040	2,550	22
IrPdReRu	none	3,600	1,120	2,640	21	IrPdRhRu	none	2,560	840	2,230	16	IrPtReRh	fcc	1,840	980	2,610	21
IrPtReRu	fcc	1,920	1,220	2,690	19	IrPtRhRu	fcc	860	560	2,400	7	MnMoNbRe	bcc	2,180	1,520	2,240	24
MnMoNbTa	none	4,140	1,660	2,320	21	MnMoNbTi	none	3,560	1,520	2,040	27	MnMoNbV	none	3,280	1,600	2,140	20
MnMoNbW	bcc	2,440	1,180	2,710	19	MnMoNbZr	none	3,140	1,780	1,930	39	MnMoNiV	none	2,020	1,260	1,800	50
MnMoReTa	none	3,160	1,760	2,300	27	MnMoReTi	none	2,400	1,520	2,040	33	MnMoReV	bcc	1,580	1,140	2,200	22
MnMoReW	bcc	1,780	1,460	2,890	24	MnMoReZr	none	2,280	2,080	1,890	45	MnMoTaTi	none	4,140	1,680	2,100	28

	S.S.	T_c	$\tilde{T}_c$	$\bar{T}_m$	CV		S.S.	T_c	$\tilde{T}_c$	$\bar{T}_m$	CV		S.S.	T_c	$\tilde{T}_c$	$\bar{T}_m$	CV
MnMoTaV	none	3,680	1,740	2,180	19	MnMoTaW	none	3,420	1,300	2,840	20	MnMoTaZr	none	3,740	1,800	1,950	45
MnMoTiV	none	3,020	1,340	1,950	25	MnMoTiW	none	3,660	1,580	2,510	25	MnMoTiZr	none	3,060	1,520	1,750	43
MnMoVW	bcc	2,500	1,160	2,560	18	MnMoVZr	none	5,000	5,000	1,800	47	MnMoWZr	none	2,580	1,920	2,550	43
MnNbNiV	none	2,840	1,420	1,670	50	MnNbReTa	none	4,900	2,080	2,270	30	MnNbReTi	none	3,900	2,000	1,990	34
MnNbReV	none	3,300	1,720	2,120	25	MnNbReW	bcc	2,460	1,200	2,850	26	MnNbReZr	none	3,940	2,120	1,890	46
MnNbTaTi	none	3,840	1,280	2,070	28	MnNbTaV	none	3,540	1,420	2,120	18	MnNbTaW	none	4,240	1,540	2,800	22
MnNbTaZr	none	4,320	1,660	1,980	39	MnNbTiV	none	2,920	1,220	1,870	26	MnNbTiW	none	3,900	1,560	2,470	28
MnNbTiZr	none	3,600	1,560	1,760	43	MnNbVW	none	3,120	1,480	2,530	19	MnNbVZr	none	3,320	1,780	1,790	40
MnNbWZr	none	3,120	1,700	2,520	47	MnNiOsPd	none	5,000	5,000	2,100	50	MnNiPdRe	none	5,000	5,000	2,130	50
MnNiPdRu	fcc	820	2,400	1,910	50	MnOsPdRe	none	5,000	5,000	2,530	44	MnOsPdRu	fcc	1,080	2,360	2,310	45
MnPdReRu	none	5,000	5,000	2,350	49	MnReTaTi	none	4,880	2,240	2,090	35	MnReTaV	none	4,380	2,000	2,190	27
MnReTaW	none	3,420	1,520	2,980	28	MnReTaZr	none	5,000	5,000	1,950	47	MnReTiV	none	3,300	1,740	1,970	30
MnReTiW	none	3,400	2,040	2,650	34	MnReTiZr	none	3,300	2,180	1,760	48	MnReVW	bcc	1,600	980	2,700	24
MnReVZr	none	3,220	2,460	1,840	46	MnReWZr	none	3,020	2,220	2,690	44	MnTaTiV	none	3,580	1,640	1,950	27
MnTaTiW	none	4,520	2,500	2,600	32	MnTaVW	none	3,680	1,760	2,660	20	MnTaVZr	none	5,000	5,000	1,820	50
MnTaWZr	none	5,000	5,000	2,650	47	MnTiVW	none	3,180	1,280	2,320	25	MnTiVZr	none	3,460	1,880	1,650	42
MnTiWZr	none	3,740	1,980	2,310	42	MnVWZr	none	3,560	1,900	2,370	47	MoNbNiV	bcc	1,740	1,140	2,100	48
MoNbReTa	none	3,320	1,500	2,870	17	MoNbReTi	bcc	1,940	1,160	2,510	23	MoNbReV	bcc	1,960	1,260	2,610	13
MoNbReW	bcc	1,780	920	2,940	11	MoNbReZr	none	2,400	1,600	2,350	24	MoNbTaTi	bcc	580	440	2,620	9
MoNbTaV	bcc	1,060	720	2,650	4	MoNbTaW	bcc	1,000	540	3,070	4	MoNbTaZr	none	3,720	2,260	2,470	14
MoNbTiV	bcc	760	640	2,310	11	MoNbTiW	bcc	760	520	2,610	13	MoNbTiZr	bcc	1,020	820	2,170	18
MoNbVW	bcc	700	500	2,710	5	MoNbVZr	bcc	2,120	1,140	2,170	16	MoNbWZr	bcc	2,280	900	2,660	14
MoNiOsPd	fcc	2,020	1,500	2,030	35	MoNiOsPt	fcc	1,280	1,340	2,190	38	MoNiPdPt	fcc	1,260	1,200	1,920	38
MoNiPdRe	fcc	1,940	1,520	2,020	37	MoNiPdRh	none	2,020	1,220	1,930	33	MoNiPdRu	none	2,240	1,320	1,910	33
MoNiPtRe	fcc	1,440	1,580	2,250	41	MoNiPtRh	fcc	760	1,140	2,070	35	MoNiPtRu	fcc	1,320	1,260	2,100	36
MoNiReV	bcc	1,620	1,120	2,210	50	MoOsPdPt	fcc	1,280	1,720	2,190	35	MoOsPdRe	fcc	1,820	1,760	2,870	27
MoOsPdRh	fcc	1,600	1,300	2,570	26	MoOsPdRu	fcc	1,780	1,620	2,650	25	MoOsPtRe	fcc	2,180	2,000	2,930	31
MoOsPtRh	fcc	1,200	1,200	2,620	29	MoOsPtRu	fcc	1,840	1,580	2,710	33	MoPdPtRe	fcc	1,000	1,380	2,290	39
MoPdPtRh	fcc	1,540	1,220	2,120	32	MoPdPtRu	fcc	1,360	1,260	2,130	34	MoPdReRh	fcc	1,820	1,460	2,310	29
MoPdReRu	fcc	1,700	1,560	2,300	26	MoPdRhRu	fcc	2,100	1,260	2,130	24	MoPtReRh	fcc	780	1,120	2,550	33
MoPtReRu	fcc	580	1,440	2,580	30	MoPtRhRu	fcc	2,100	1,220	2,320	28	MoReTaTi	none	2,740	1,440	2,620	25
MoReTaV	none	2,700	1,500	2,700	16	MoReTaW	bcc	2,620	1,120	3,090	14	MoReTaZr	none	3,820	2,280	2,430	32
MoReTiV	bcc	1,300	1,220	2,390	23	MoReTiW	bcc	2,440	1,400	2,660	24	MoReTiZr	bcc	1,820	1,340	2,150	30
MoReVW	bcc	1,360	900	2,810	10	MoReVZr	none	2,320	1,800	2,200	27	MoReWZr	bcc	2,280	1,780	2,660	23
MoTaTiV	bcc	760	920	2,410	11	MoTaTiW	bcc	980	620	2,770	13	MoTaTiZr	bcc	1,500	1,040	2,250	18
MoTaVW	bcc	1,140	900	2,840	5	MoTaVZr	none	5,000	5,000	2,220	20	MoTaWZr	bcc	2,760	1,340	2,780	14
MoTiVW	bcc	860	600	2,440	14	MoTiVZr	bcc	1,720	1,080	1,970	22	MoTiWZr	bcc	1,900	1,180	2,400	21
MoVWZr	none	3,440	1,180	2,450	21	NbPdPtRh	fcc	220	2,640	2,210	45	NbPdRhRu	none	5,000	5,000	2,350	49
NbPtRhRu	none	5,000	5,000	2,400	50	NbReTaTi	bcc	880	980	2,590	24	NbReTaV	bcc	1,360	1,120	2,640	17
NbReTaW	bcc	2,940	1,220	3,020	18	NbReTaZr	bcc	1,440	1,260	2,450	26	NbReTiV	bcc	1,040	1,020	2,320	22
NbReTiW	bcc	1,620	1,180	2,580	25	NbReTiZr	bcc	1,040	1,120	2,160	29	NbReVW	bcc	1,420	1,100	2,700	15
NbReVZr	bcc	2,180	1,400	2,190	27	NbReWZr	bcc	2,000	1,520	2,640	25	NbTaTiV	bcc	980	800	2,350	6
NbTaTiW	bcc	380	320	2,700	9	NbTaTiZr	bcc	880	700	2,270	12	NbTaVW	bcc	920	440	2,750	5
NbTaVZr	bcc	1,680	1,240	2,220	11	NbTaWZr	bcc	1,980	1,160	2,770	12	NbTiVW	bcc	780	580	2,330	10
NbTiVZr	bcc	1,400	1,120	1,960	16	NbTiWZr	bcc	1,660	860	2,380	16	NbVWZr	none	3,100	1,300	2,400	18
NiOsPdPt	none	1,940	1,280	1,880	19	NiOsPdRe	fcc	1,560	1,660	2,580	27	NiOsPdRh	fcc	1,220	1,160	2,280	19
NiOsPdRu	fcc	960	1,520	2,360	28	NiOsPtRe	fcc	1,040	1,340	2,640	29	NiOsPtRh	fcc	1,780	1,040	2,330	17
NiOsPtRu	fcc	1,920	1,320	2,420	18	NiPdPtRe	fcc	1,160	1,100	1,930	28	NiPdPtRh	fcc	1,560	680	1,830	10
NiPdPtRu	fcc	1,160	920	1,850	14	NiPdReRh	fcc	1,460	1,340	1,990	24	NiPdReRu	fcc	820	1,420	1,990	24
NiPdRhRu	fcc	960	920	1,880	19	NiPtReRh	fcc	1,380	940	2,200	26	NiPtReRu	fcc	1,340	1,040	2,240	26
NiPtRhRu	fcc	1,480	740	2,050	12	OsPdPtRe	fcc	1,460	1,680	2,660	28	OsPdPtRh	fcc	1,340	1,020	2,360	17
OsPdPtRu	fcc	580	1,340	2,440	21	OsPdReRh	fcc	2,640	1,040	2,710	23	OsPdReRu	fcc	740	1,400	2,800	20
OsPdRhRu	none	5,000	5,000	2,490	15	OsPtReRh	fcc	1,660	980	2,760	23	OsPtReRu	fcc	1,780	1,020	2,850	19

	S.S.	T_c	$\tilde{T}_c$	$\bar{T}_m$	CV		S.S.	T_c	$\tilde{T}_c$	$\bar{T}_m$	CV		S.S.	T_c	$\tilde{T}_c$	$\bar{T}_m$	CV
OsPtRhRu	fcc	1,500	860	2,550	12	PdPtReRh	fcc	1,680	1,000	2,240	26	PdPtReRu	fcc	1,560	1,320	2,270	25
PdPtRhRu	fcc	840	800	2,090	12	PdReRhRu	none	2,600	900	2,310	20	PtReRhRu	fcc	1,680	840	2,570	21
ReTaTiV	bcc	1,080	1,160	2,440	24	ReTaTiW	bcc	2,080	1,300	2,760	26	ReTaTiZr	bcc	1,460	1,460	2,260	30
ReTaVW	bcc	2,320	1,280	2,870	18	ReTaVZr	bcc	2,240	1,640	2,270	29	ReTaWZr	none	2,940	1,940	2,780	27
ReTiVW	bcc	1,420	1,240	2,470	24	ReTiVZr	none	2,040	1,440	2,030	30	ReTiWZr	bcc	1,820	1,800	2,420	31
ReVWZr	bcc	2,460	1,700	2,490	29	TaTiVW	bcc	720	800	2,490	10	TaTiVZr	bcc	1,220	1,440	2,040	16
TaTiWZr	bcc	2,040	1,080	2,530	16	TaVWZr	none	3,520	1,560	2,530	18	TiVWZr	none	2,540	1,260	2,190	21

D. Quinary alloys at equi-composition

TABLE VI: LTVC results for quinary alloys. S.S. type of single solid solution phase ("none" = not found); T_c (K) transition temperature, as estimated by the method; $\tilde{T}_c$ (K) approximated transition temperature, estimated according to Eq. (8); CV (meV) cluster expansion cross validation score; $\bar{T}_m$ (K) melting temperature (solidus), calculated as the average of the melting temperatures at equi-composition of the 10 binary alloys associated with the quinary alloy; A solid solution is predicted if $T_c < \bar{T}_m$.

	S.S.	T_c	$\tilde{T}_c$	$\bar{T}_m$	CV		S.S.	T_c	$\tilde{T}_c$	$\bar{T}_m$	CV
AlCrMoTiW	bcc	1,650	1,000	2,150	44	CoCrFeMnNi	fcc	850	950	1,640	43
CrHfMoNbTa	bcc	1,900	1,250	2,440	19	CrHfMoNbTi	bcc	1,700	1,100	2,180	23
CrHfMoNbV	none	2,550	1,150	2,230	21	CrHfMoNbW	bcc	2,100	1,000	2,520	19
CrHfMoNbZr	bcc	1,800	1,450	2,150	26	CrHfMoTaTi	bcc	1,650	1,250	2,260	23
CrHfMoTaV	none	2,300	1,150	2,290	22	CrHfMoTaW	bcc	1,900	1,100	2,620	19
CrHfMoTaZr	bcc	2,050	1,600	2,200	26	CrHfMoTiV	none	2,200	1,100	2,060	26
CrHfMoTiW	bcc	1,750	1,000	2,320	24	CrHfMoTiZr	bcc	1,750	1,350	1,990	30
CrHfMoVW	bcc	2,300	1,150	2,390	22	CrHfMoVZr	none	3,000	1,450	2,000	30
CrHfMoWZr	bcc	1,750	1,100	2,380	27	CrHfNbTaTi	bcc	1,450	1,100	2,240	21
CrHfNbTaV	none	2,350	1,000	2,260	20	CrHfNbTaW	bcc	1,650	850	2,590	18
CrHfNbTaZr	none	5,000	5000	2,220	31	CrHfNbTiV	none	2,250	1,000	2,020	24
CrHfNbTiW	bcc	1,450	850	2,270	22	CrHfNbTiZr	bcc	1,700	1,300	2,000	27
CrHfNbVW	bcc	2,200	1,000	2,330	20	CrHfNbVZr	none	3,400	1,500	2,000	28
CrHfNbWZr	bcc	1,700	1,150	2,370	25	CrHfTaTiV	bcc	1,600	1,050	2,100	24
CrHfTaTiW	bcc	1,200	900	2,390	22	CrHfTaTiZr	bcc	1,700	1,450	2,070	27
CrHfTaVW	bcc	1,800	1,050	2,430	21	CrHfTaVZr	none	2,750	1,350	2,050	28
CrHfTaWZr	bcc	2,250	1,200	2,460	25	CrHfTiVW	bcc	1,650	1,000	2,150	24
CrHfTiVZr	none	2,850	1,250	1,870	31	CrHfTiWZr	bcc	1,750	1,150	2,200	28
CrHfVWZr	none	3,050	1,400	2,230	29	CrMoNbTaTi	bcc	1,650	900	2,390	12
CrMoNbTaV	bcc	2,350	900	2,440	8	CrMoNbTaW	none	2,750	900	2,740	8
CrMoNbTaZr	none	2,900	1,400	2,290	22	CrMoNbTiV	bcc	1,900	800	2,180	12
CrMoNbTiW	bcc	1,900	750	2,410	13	CrMoNbTiZr	bcc	1,900	1,150	2,050	21
CrMoNbVW	bcc	2,050	750	2,510	6	CrMoNbVZr	none	3,050	1,250	2,090	20
CrMoNbWZr	none	3,050	1,400	2,430	22	CrMoTaTiV	bcc	1,700	800	2,270	12
CrMoTaTiW	bcc	1,600	800	2,540	13	CrMoTaTiZr	none	2,150	1,300	2,130	21
CrMoTaVW	bcc	2,000	850	2,620	7	CrMoTaVZr	none	3,450	1,400	2,150	20
CrMoTaWZr	none	2,750	1,450	2,540	26	CrMoTiVW	bcc	1,600	800	2,320	13
CrMoTiVZr	none	2,800	1,200	1,950	24	CrMoTiWZr	none	2,500	1,050	2,250	22
CrMoVWZr	none	3,900	1,200	2,320	21	CrNbTaTiV	bcc	1,800	700	2,200	11
CrNbTaTiW	bcc	1,550	650	2,460	12	CrNbTaTiZr	bcc	1,800	1,150	2,110	19
CrNbTaVW	bcc	2,150	800	2,530	7	CrNbTaVZr	none	2,850	1,300	2,120	22
CrNbTaWZr	none	2,650	1,350	2,500	18	CrNbTiVW	bcc	1,750	700	2,220	12
CrNbTiVZr	none	2,500	1,050	1,900	22	CrNbTiWZr	none	2,250	1,000	2,200	20

	S.S.	T_c	$\bar{T}_c$	$\bar{T}_m$	CV		S.S.	T_c	$\bar{T}_c$	$\bar{T}_m$	CV
CrNbVWZr	none	3,000	1,450	2,260	21	CrTaTiVW	bcc	1,400	700	2,360	12
CrTaTiVZr	none	2,350	1,100	1,990	22	CrTaTiWZr	none	2,550	1,050	2,330	20
CrTaVWZr	none	3,300	1,600	2,370	24	CrTiVWZr	none	3,400	1,200	2,110	23
HfMoNbTaTi	bcc	1,250	700	2,480	17	HfMoNbTaV	bcc	1,300	700	2,480	15
HfMoNbTaW	bcc	1,450	650	2,830	14	HfMoNbTaZr	bcc	1,250	900	2,420	17
HfMoNbTiV	bcc	1,400	800	2,230	20	HfMoNbTiW	bcc	1,200	650	2,510	19
HfMoNbTiZr	bcc	1,400	800	2,190	22	HfMoNbVW	bcc	1,600	750	2,550	17
HfMoNbVZr	bcc	1,450	850	2,170	22	HfMoNbWZr	bcc	1,400	850	2,570	20
HfMoTaTiV	bcc	1,450	850	2,280	20	HfMoTaTiW	bcc	1,350	750	2,600	19
HfMoTaTiZr	bcc	1,600	950	2,240	22	HfMoTaVW	bcc	1,650	800	2,620	17
HfMoTaVZr	bcc	1,600	950	2,200	22	HfMoTaWZr	bcc	1,850	950	2,630	19
HfMoTiVW	bcc	1,550	800	2,330	22	HfMoTiVZr	bcc	1,800	1,050	2,000	26
HfMoTiWZr	bcc	1,350	850	2,360	25	HfMoVWZr	bcc	2,150	1,150	2,370	25
HfNbTaTiV	bcc	1,300	750	2,280	16	HfNbTaTiW	bcc	1,250	650	2,590	15
HfNbTaTiZr	bcc	1,300	750	2,280	17	HfNbTaVW	bcc	1,150	650	2,600	14
HfNbTaVZr	bcc	1,650	900	2,230	16	HfNbTaWZr	bcc	1,750	700	2,660	16
HfNbTiVW	bcc	1,450	750	2,300	18	HfNbTiVZr	bcc	1,750	900	2,020	21
HfNbTiWZr	bcc	1,600	750	2,380	20	HfNbVWZr	bcc	2,200	950	2,370	21
HfTaTiVW	bcc	1,600	800	2,390	17	HfTaTiVZr	none	2,750	1,400	2,070	23
HfTaTiWZr	bcc	1,950	900	2,460	20	HfTaVWZr	bcc	2,250	1,050	2,440	21
HfTiVWZr	none	2,300	1,050	2,190	23	MoNbReTaW	bcc	2,750	1,100	3,000	14
MoNbTaTiV	bcc	800	450	2,470	8	MoNbTaTiW	bcc	750	450	2,750	10
MoNbTaTiZr	bcc	1,350	700	2,360	13	MoNbTaVW	bcc	1,000	500	2,800	5
MoNbTaVZr	none	3,550	1,100	2,350	14	MoNbTaWZr	bcc	2,650	850	2,750	11
MoNbTiVW	bcc	750	450	2,480	11	MoNbTiVZr	bcc	1,450	700	2,120	17
MoNbTiWZr	bcc	1,850	700	2,450	16	MoNbVWZr	none	3,050	900	2,480	16
MoTaTiVW	bcc	850	500	2,590	11	MoTaTiVZr	bcc	1,750	800	2,180	17
MoTaTiWZr	bcc	2,150	850	2,540	17	MoTaVWZr	none	3,400	1,050	2,560	17
MoTiVWZr	none	2,550	950	2,290	20	NbReTaTiV	bcc	950	800	2,470	19
NbTaTiVW	bcc	800	400	2,520	8	NbTaTiVZr	none	3,100	1,150	2,170	15
NbTaTiWZr	bcc	1,800	600	2,530	13	NbTaVWZr	none	2,850	850	2,530	14
NbTiVWZr	bcc	2,050	750	2,250	17	TaTiVWZr	none	2,400	800	2,350	17

[1] J.-W. Yeh, S.-K. Chen, S.-J. Lin, J.-Y. Gan, T.-S. Chin, T.-T. Shun, C.-H. Tsau, and S.-Y. Chang, *Nanostructured High-Entropy Alloys with Multiple Principle Elements: Novel Alloy Design Concepts and Outcomes*, Adv. Eng. Mater. **6**, 299–303 (2004).

[2] B. Cantor, I. T. H. Chang, P. Knight, and A. J. B. Vincent, *Microstructural development in equiatomic multicomponent alloys*, Mater. Sci. Eng. A **375**, 213–218 (2004).

[3] O. N. Senkov, J. D. Miller, D. B. Miracle, and C. Woodward, *Accelerated exploration of multi-principal element alloys with solid solution phases*, Nature Commun. **6**, 6529 (2015).

[4] S. Gorsse, D. B. Miracle, and O. N. Senkov, *Mapping the world of complex concentrated alloys*, Acta Mater. **135**, 177–187 (2017).

[5] X. Lim, *Mixed-up metals make for stronger, tougher, stretchier alloys*, Naturere **533**, 306–307 (2016).

[6] B. Gludovatz, A. Hohenwarter, D. Catoor, E. H. Chang, E. P. George, and R. O. Ritchie, *A fracture-resistant high-entropy alloy for cryogenic applications*, Science **345**, 1153–1158 (2014).

[7] F. von Rohr, M. J. Winiarski, J. Tao, T. Klimczuk, and R. J. Cava, *Effect of electron count and chemical complexity in the Ta-Nb-Hf-Zr-Ti high-entropy alloy superconductor*, Proc. Nature. Acad. Sci. **113**, E7144–E7150 (2016).

[8] Z. Li, K. G. Pradeep, Y. Deng, D. Raabe, and C. C. Tasan, *Metastable high-entropy dual-phase alloys overcome the strength-ductility trade-off*, Naturere **534**, 227–

230 (2016).

[9] J.-W. Yeh, A.-C. Yeh, and S.-Y. Chang, *Potential Applications and Prospects*, in *High-Entropy Alloys: Fundamentals and Applications*, edited by M. C. Gao, J.-W. Yeh, P. K. Liaw, and Y. Zhang (Springer, Cham, Switzerland, 2015), chap. 15.

[10] C. M. Rost, E. Sachet, T. Borman, A. Moballegh, E. C. Dickey, D. Hou, J. L. Jones, S. Curtarolo, and J.-P. Maria, *Entropy-stabilized oxides*, Nature Commun. **6**, 8485 (2015).

[11] S. Guo and C. T. Liu, *Phase stability in high entropy alloys: Formation of solid-solution phase or amorphous phase*, Prog. Nature Sci. Mater. Int. **21**, 433–446 (2011).

[12] Y. Zhang, S. Guo, C. T. Liu, and X. Yang, *Phase Formation Rules*, in *High-Entropy Alloys: Fundamentals and Applications*, edited by M. C. Gao, J.-W. Yeh, P. K. Liaw, and Y. Zhang (Springer, Cham, Switzerland, 2015), chap. 2.

[13] M. C. Gao, *Design of High-Entropy Alloys*, in *High-Entropy Alloys: Fundamentals and Applications*, edited by M. C. Gao, J.-W. Yeh, P. K. Liaw, and Y. Zhang (Springer, Cham, Switzerland, 2015), chap. 11.

[14] Y. Zhang, Y. J. Zhou, J. P. Lin, G. L. Chen, and P. K. Liaw, *Solid-Solution Phase Formation Rules for Multi-component Alloys*, Adv. Eng. Mater. **10**, 534–538 (2008).

[15] M. G. Poletti and L. Battezatti, *Electronic and thermodynamic criteria for the occurrence of high entropy alloys in metallic systems*, Acta Mater. **75**, 297–306 (2014).

[16] Y. F. Ye, C. T. Liu, and Y. Yang, *A geometric model for intrinsic residual strain and phase stability in high entropy alloys*, Acta Mater. **94**, 152–161 (2015).

[17] Y. F. Ye, Q. Wang, J. Lu, C. T. Liu, and Y. Yang, *Design of high entropy alloys: A single parameter thermodynamic rule*, Scr. Mater. **104**, 53–55 (2015).

[18] S. Guo, C. Ng, Z. Wang, and C. T. Liu, *Solid solutioning in equiatomic alloys: Limit set by topological instability*, J. Alloys Compd. **583**, 410–413 (2014).

[19] S. Guo, C. Ng, J. Lu, and C. T. Liu, *Effect of valence electron concentration on stability of fcc or bcc phase in high entropy alloys*, J. Appl. Phys. **109**, 103505 (2011).

[20] M. C. Troparevsky, J. R. Morris, P. R. C. Kent, A. R. Lupini, and G. M. Stocks, *Criteria for Predicting the Formation of Single-Phase High-Entropy Alloys*, Phys. Rev. X **5**, 011041 (2015).

[21] M. C. Gao and D. E. Alman, *Searching for Next Single-Phase High-Entropy Alloy Compositions*, Entropy **15**, 4504–4519 (2013).

[22] F. Zhang, C. Zhang, S. L. Chen, J. Zhu, W. S. Cao, and U. R. Kattner, *An understanding of high entropy alloys from phase diagram calculations*, Calphad **45**, 1–10 (2014).

[23] M. Widom, *Prediction of Structure and Phase Transformations*, in *High-Entropy Alloys: Fundamentals and Applications*, edited by M. C. Gao, J.-W. Yeh, P. K. Liaw, and Y. Zhang (Springer, Cham, Switzerland, 2015), chap. 8.

[24] W. P. Huhn and M. Widom, *Prediction of A2 to B2 Phase Transition in the High Entropy Alloy Mo-Nb-Ta-W*, JOM **65**, 1772–1779 (2013).

[25] M. Widom, *Entropy and diffuse scattering: comparison of NbTiVZr and CrMoNbV*, Metall. Mater. Trans. A **47**, 3306–3311 (2016).

[26] D. de Fontaine, *Cluster Approach to Order-Disorder Transformations in Alloys*, in *Solid State Physics*, edited by H. Ehrenreich and D. Turnbull (Wiley, New York, 1994), vol. 47, pp. 33–176.

[27] A. van de Walle and M. Asta, *Self-driven lattice-model Monte Carlo simulations of alloy thermodynamic properties and phase diagrams*, Modelling Simul. Mater. Sci. Eng. **10**, 521 (2002).

[28] S. Curtarolo, G. L. W. Hart, M. Buongiorno Nardelli, N. Mingo, S. Sanvito, and O. Levy, *The high-throughput highway to computational materials design*, Nature Mater. **12**, 191–201 (2013).

[29] S. Curtarolo, W. Setyawan, G. L. W. Hart, M. Jahnátek, R. V. Chepulskii, R. H. Taylor, S. Wang, J. Xue, K. Yang, O. Levy, M. J. Mehl, H. T. Stokes, D. O. Demchenko, and D. Morgan, *AFLOW: An automatic framework for high-throughput materials discovery*, Comput. Mater. Sci. **58**, 218–226 (2012).

[30] W. Setyawan and S. Curtarolo, *High-throughput electronic band structure calculations: Challenges and tools*, Comput. Mater. Sci. **49**, 299–312 (2010).

[31] K. Yang, C. Oses, and S. Curtarolo, *Modeling Off-Stoichiometry Materials with a High-Throughput Ab-Initio Approach*, Chem. Mater. **28**, 6484–6492 (2016).

[32] O. Levy, M. Jahnátek, R. V. Chepulskii, G. L. W. Hart, and S. Curtarolo, *Ordered Structures in Rhenium Binary Alloys from First-Principles Calculations*, J. Am. Chem. Soc. **133**, 158–163 (2011).

[33] O. Levy, G. L. W. Hart, and S. Curtarolo, *Structure maps for hcp metals from first-principles calculations*, Phys. Rev. B **81**, 174106 (2010).

[34] O. Levy, G. L. W. Hart, and S. Curtarolo, *Uncovering Compounds by Synergy of Cluster Expansion and High-Throughput Methods*, J. Am. Chem. Soc. **132**, 4830–4833 (2010).

[35] G. L. W. Hart, S. Curtarolo, T. B. Massalski, and O. Levy, *Comprehensive Search for New Phases and Compounds in Binary Alloy Systems Based on Platinum-Group Metals, Using a Computational First-Principles Approach*, Phys. Rev. X **3**, 041035 (2013).

[36] M. J. Mehl, D. Hicks, C. Toher, O. Levy, R. M. Hanson, G. L. W. Hart, and S. Curtarolo, *The AFLOW Library of Crystallographic Prototypes: Part 1*, Comput. Mater. Sci. **136**, S1–S828 (2017).

[37] S. Curtarolo, W. Setyawan, S. Wang, J. Xue, K. Yang, R. H. Taylor, L. J. Nelson, G. L. W. Hart, S. Sanvito, M. Buongiorno Nardelli, N. Mingo, and O. Levy, *AFLOWLIB.ORG: A distributed materials properties repository from high-throughput ab initio calculations*, Comput. Mater. Sci. **58**, 227–235 (2012).

[38] R. H. Taylor, F. Rose, C. Toher, O. Levy, K. Yang, M. Buongiorno Nardelli, and S. Curtarolo, *A RESTful API for exchanging materials data in the AFLOWLIB.org consortium*, Comput. Mater. Sci. **93**, 178–192 (2014).

[39] C. E. Calderon, J. J. Plata, C. Toher, C. Oses, O. Levy, M. Fornari, A. Naturen, M. J. Mehl, G. L. W. Hart, M. Buongiorno Nardelli, and S. Curtarolo, *The AFLOW standard for high-throughput materials science calculations*, Comput. Mater. Sci. **108 Part A**, 233–238 (2015).

[40] F. Rose, C. Toher, E. Gossett, C. Oses, M. Buongiorno Nardelli, M. Fornari, and S. Curtarolo, *AFLUX: The LUX materials search API for the AFLOW data repositories*, Comput. Mater. Sci. **137**, 362–370 (2017).

[41] J. M. Sanchez, F. Ducastelle, and D. Gratias, *Generalized cluster description of multicomponent systems*, Physica A

128, 334–350 (1984).

[42] A. van de Walle, M. Asta, and G. Ceder, *The Alloy Theoretic Automated Toolkit: A User Guide*, Calphad **26**, 539–553 (2002).

[43] A. Sher, M. van Schilfgaarde, A.-B. Chen, and W. Chen, *Quasichemical approximation in binary alloys*, Phys. Rev. B **36**, 4279 (1987).

[44] M. A. Berding and A. Sher, *Electronic quasichemical formalism: Application to arsenic deactivation in silicon*, Phys. Rev. B **58**, 3853 (1998).

[45] T. B. Massalski, H. Okamoto, P. R. Subramanian, and L. Kacprzak, eds., *Binary Alloy Phase Diagrams* (American Society for Metals, Materials Park, OH, 1990).

[46] J.-O. Andersson, T. Helander, L. Höglund, P. Shi, and B. Sundman, *Thermo-Calc & DICTRA, computational tools for materials science*, Calphad **26**, 273–312 (2002).

[47] Thermo-Calc Software, *Thermo-Calc Software Database SSOL version 5*, http://www.thermocalc.com/products-services/software/thermo-calc/ (2015).

[48] Z. Wu, H. Bei, F. Otto, G. M. Pharr, and E. P. George, *Recovery, recrystallization, grain growth and phase stability of a family of FCC-structured multi-component equiatomic solid solution alloys*, Intermetallics **46**, 131–140 (2014).

[49] M. S. Lucas, G. B. Wilks, L. Mauger, J. A. Muñoz, O. N. Senkov, E. Michel, J. Horwath, S. L. Semiatin, M. B. Stone, D. L. Abernathy, and E. Karapetrova, *Absence of long-range chemical ordering in equimolar FeCoCrNi*, Appl. Phys. Lett. **100**, 251907 (2012).

[50] R. Kozak, A. Sologubenko, and W. Steurer, *Single-phase high-entropy alloys - an overview*, Zeitschrift für Kristallographie - Crystalline Materials **230**, 55 (2015).

[51] N. D. Stepanov, D. G. Shaysultanov, G. A. Salishchev, and M. A. Tikhonovsky, *Structure and mechanical properties of a light-weight AlNbTiV high entropy alloy*, Mater. Lett. **142**, 153–155 (2015).

[52] Y. D. Wu, Y. H. Cai, T. Wang, J. J. Si, J. Zhu, Y. D. Wang, and X. D. Hui, *A refractory $Hf_{25}Nb_{25}Ti_{25}Zr_{25}$ high-entropy alloy with excellent structural stability and tensile properties*, Mater. Lett. **130**, 277–280 (2014).

[53] O. N. Senkov, G. B. Wilks, D. B. Miracle, C. P. Chuang, and P. K. Liaw, *Refractory high-entropy alloys*, Intermetallics **18**, 1758–1765 (2010).

[54] O. N. Senkov, G. B. Wilks, J. M. Scott, and D. B. Miracle, *Mechanical properties of $Nb_{25}Mo_{25}Ta_{25}W_{25}$ and $V_{20}Nb_{20}Mo_{20}Ta_{20}W_{20}$ refractory high entropy alloys*, Intermetallics **19**, 698–706 (2011).

[55] X. Yang, Y. Zhang, and P. K. Liaw, *Microstructure and Compressive Properties of $NbTiVTaAl_x$ High Entropy Alloys*, Procedia Engineering **36**, 292–298 (2012).

[56] O. N. Senkov, S. V. Senkova, D. B. Miracle, and C. Woodward, *Mechanical properties of low-density, refractory multi-principal element alloys of the Cr-Nb-Ti-V-Zr system*, Mater. Sci. Eng. A **565**, 51–62 (2013).

[57] Y. Zhang, X. Yang, and P. K. Liaw, *Alloy design and properties optimization of high-entropy alloys*, JOM **64**, 830–838 (2012).

[58] B. Gorr, M. Azim, H.-J. Christ, T. Mueller, D. Schliephake, and M. Heilmaier, *Phase equilibria, microstructure, and high temperature oxidation resistance of novel refractory high-entropy alloys*, J. Alloys Compd. **624**, 270–278 (2015).

[59] O. N. Senkov, J. M. Scott, S. V. Senkova, D. B. Miracle, and C. F. Woodward, *Microstructure and room temperature properties of a high-entropy TaNbHfZrTi alloy*, J. Alloys Compd. **509**, 6043–6048 (2011).

[60] H. Bei, *Multi-component solid solution alloys having high mixing entropy*, USA Patent US **A1**, 0108502 (2013).

[61] M. C. Gao, B. Zhang, S. Yang, and S. M. Guo, *Senary Refractory High-Entropy Alloy HfNbTaTiVZr*, Metall. Mater. Trans. A **47**, 3333–3345 (2016).

[62] G. L. W. Hart and R. W. Forcade, *Algorithm for generating derivative structures*, Phys. Rev. B **77**, 224115 (2008).

[63] G. L. W. Hart and R. W. Forcade, *Generating derivative structures from multilattices: Algorithm and application to hcp alloys*, Phys. Rev. B **80**, 014120 (2009).

[64] A. van de Walle, *Multicomponent multisublattice alloys, nonconfigurational entropy and other additions to the Alloy Theoretic Automated Toolkit*, Calphad **33**, 266 (2009).

[65] G. Kresse and J. Furthmüller, *Efficient iterative schemes for ab initio total-energy calculations using a plane-wave basis set*, Phys. Rev. B **54**, 11169–11186 (1996).

[66] C. Toher, J. J. Plata, O. Levy, M. de Jong, M. D. Asta, M. Buongiorno Nardelli, and S. Curtarolo, *High-throughput computational screening of thermal conductivity, Debye temperature, and Grüneisen parameter using a quasiharmonic Debye model*, Phys. Rev. B **90**, 174107 (2014).

[67] C. Toher, C. Oses, J. J. Plata, D. Hicks, F. Rose, O. Levy, M. de Jong, M. D. Asta, M. Fornari, M. Buongiorno Nardelli, and S. Curtarolo, *Combining the AFLOW GIBBS and Elastic Libraries to efficiently and robustly screen thermomechanical properties of solids*, Phys. Rev. Mater. **1**, 015401 (2017).

[68] R. Kikuchi, *A Theory of Cooperative Phenomena*, Phys. Rev. **81**, 988 (1951).

[69] S. Kullback and R. A. Leibler, *On Information and Sufficiency*, Ann. Math. Stat. **22**, 79–86 (1951).

[70] V. Vedral, *The role of relative entropy in quantum information theory*, Rev. Mod. Phys. **74**, 197 (2002).

[71] H. Qian, *Relative entropy: Free energy associated with equilibrium fluctuations and nonequilibrium deviations*, Phys. Rev. E **63**, 042103 (2001).

[72] J. Kristensen, I. Bilionis, and N. Zabaras, *Relative entropy as model selection tool in cluster expansion*, Phys. Rev. B **87**, 174112 (2013).

[73] C. Nyshadham, C. Oses, J. E. Hansen, I. Takeuchi, S. Curtarolo, and G. L. W. Hart, *A computational high-throughput search for new ternary superalloys*, Acta Mater. **122**, 438–447 (2017).

[74] V. Ozolins, C. Wolverton, and A. Zunger, *Cu-Au, Ag-Au, Cu-Ag, and Ni-Au intermetallics: First-principles study of temperature-composition phase diagrams and structures*, Phys. Rev. B **57**, 6427 (1998).